

RESEARCH ARTICLE

# *Bacillus thuringiensis* Crystal Protein Cry6Aa Triggers *Caenorhabditis elegans* Necrosis Pathway Mediated by Aspartic Protease (ASP-1)

Fengjuan Zhang<sup>1,2</sup>, Donghai Peng<sup>1</sup>, Chunsheng Cheng<sup>1</sup>, Wei Zhou<sup>1</sup>, Shouyong Ju<sup>1</sup>, Danfeng Wan<sup>1</sup>, Ziquan Yu<sup>1</sup>, Jianwei Shi<sup>1</sup>, Yaoyao Deng<sup>1</sup>, Fenshan Wang<sup>1</sup>, Xiaobo Ye<sup>1</sup>, Zhenfei Hu<sup>1</sup>, Jian Lin<sup>1</sup>, Lifang Ruan<sup>1</sup>, Ming Sun<sup>1\*</sup>

**1** State Key Laboratory of Agricultural Microbiology, College of Life Science and Technology, Huazhong Agricultural University, Wuhan, China, **2** Haikou Experimental Station, Chinese Academy of Tropical Agricultural Sciences, Haikou, China

\* [m98sun@mail.hzau.edu.cn](mailto:m98sun@mail.hzau.edu.cn)



CrossMark  
click for updates

## OPEN ACCESS

**Citation:** Zhang F, Peng D, Cheng C, Zhou W, Ju S, Wan D, et al. (2016) *Bacillus thuringiensis* Crystal Protein Cry6Aa Triggers *Caenorhabditis elegans* Necrosis Pathway Mediated by Aspartic Protease (ASP-1). PLoS Pathog 12(1): e1005389. doi:10.1371/journal.ppat.1005389

**Editor:** David S. Schneider, Stanford University, UNITED STATES

**Received:** July 22, 2015

**Accepted:** December 18, 2015

**Published:** January 21, 2016

**Copyright:** © 2016 Zhang et al. This is an open access article distributed under the terms of the [Creative Commons Attribution License](https://creativecommons.org/licenses/by/4.0/), which permits unrestricted use, distribution, and reproduction in any medium, provided the original author and source are credited.

**Data Availability Statement:** All relevant data are within the paper and its Supporting Information files.

**Funding:** MS was supported by the National High Technology Research and Development Program (863) of China (2011AA10A203), China 948 Program of Ministry of Agriculture (2011-G25), and the National Natural Science Foundation of China (31170047). LR was supported by the National Natural Science Foundation of China (31171901). FZ was supported by State Key Laboratory of Agricultural Microbiology Program (AMLKF201306). The funders had no role in study design, data

## Abstract

Cell death plays an important role in host-pathogen interactions. Crystal proteins (toxins) are essential components of *Bacillus thuringiensis* (Bt) biological pesticides because of their specific toxicity against insects and nematodes. However, the mode of action by which crystal toxins to induce cell death is not completely understood. Here we show that crystal toxin triggers cell death by necrosis signaling pathway using crystal toxin Cry6Aa-*Caenorhabditis elegans* toxin-host interaction system, which involves an increase in concentrations of cytoplasmic calcium, lysosomal lyses, uptake of propidium iodide, and burst of death fluorescence. We find that a deficiency in the necrosis pathway confers tolerance to Cry6Aa toxin. Intriguingly, the necrosis pathway is specifically triggered by Cry6Aa, not by Cry5Ba, whose amino acid sequence is different from that of Cry6Aa. Furthermore, Cry6Aa-induced necrosis pathway requires aspartic protease (ASP-1). In addition, ASP-1 protects Cry6Aa from over-degradation in *C. elegans*. This is the first demonstration that deficiency in necrosis pathway confers tolerance to Bt crystal protein, and that Cry6A triggers necrosis represents a newly added necrosis paradigm in the *C. elegans*. Understanding this model could lead to new strategies for nematode control.

## Author Summary

Necrosis contributes to many devastating pathological conditions, such as neurodegenerative diseases and microbial pathogenesis. *Bacillus thuringiensis* crystal proteins are effective biopesticides. Our study reveals that *B. thuringiensis* Cry6Aa protein triggers the necrosis pathway using *Caenorhabditis elegans* as a model. We show that aspartic protease ASP-1 is required for Cry6Aa protein-induced necrosis, whereas intrinsic insults induce necrosis mediated by ASP-3 and ASP-4. Our findings contribute to the understanding of

collection and analysis, decision to publish, or preparation of the manuscript.

**Competing Interests:** The authors have declared that no competing interests exist.

the mechanism of Bt crystal protein action and host-pathogen interactions. Because necrosis mechanisms are conserved from nematodes to humans, the fact that necrosis can be induced by Cry6Aa provides a model system for studying necrosis mechanisms in human diseases.

## Introduction

Cell death plays critical roles in development and in pathological conditions. Apoptosis and necrosis are the two major modes of cell death [1]. Apoptosis, the most well-known mode of the cell death, plays a significant role in development, tissue homeostasis, and host defense [2,3]. Unlike apoptosis, necrosis is characterized by loss of plasma membrane integrity [4,5]. Necrotic cell death can contribute to many pathological conditions, such as inflammation [6], human neurodegenerative and aging-associated diseases [5,7]. Moreover, Necrosis plays an important role in microbial pathogenesis. In some cases, necrosis plays a significant role in antiviral/antibacterial host defense [2,8]; in others, necrosis is utilized as pathogen survival strategy to aid its spread [2].

*Bacillus thuringiensis* (Bt) is one member of the *Bacillus cereus* group of bacteria [9]. An important characteristic of Bt strains is that they produce insecticidal crystal proteins (Cry) during the sporulation phase. These proteins are highly specific to their target insects and nematodes and are harmless to non-target animals and humans, thus, they represent a viable alternative for the control of pests in agriculture and of important disease vectors in human public health [10].

The classical pore-forming model remains the widely accepted mode of action of the three-domain crystal protein (3d-Cry). When susceptible larvae ingest the 3d-Cry protoxin, it is activated by gut proteases. Upon activated toxin binding to cadherin receptor, toxins form oligomers. Subsequently, these oligomers bind to a second group of receptor proteins. Finally, they generate toxin pores in the cell membrane that lead to midgut cells lysis [10–13]. There is little information on the cellular mechanisms of the classical pore-forming model. An alternative signaling pathway model of the 3d-Cry action has also been reported. This model disregards pore formation and proposed that crystal toxins activate a  $Mg^{2+}$ -dependent adenylyl cyclase (AC)/protein kinase A (PKA) signaling pathway by interacting with receptor [14,15]. Nevertheless, this signaling pathway has only been identified in one insect cell line. There is no published data showing a signaling pathway involved in whole larvae death and the mode of action by which crystal toxins induce cell death is not completely understood.

Crystal proteins have also been shown to intoxicate nematode parasites of animals [16] and plants [17–19]. Nematicidal activity has been found in several families of Bt crystal proteins, including Cry5, Cry6, Cry12, Cry13, Cry14, Cry21, and Cry55 [17]. Cry5Ba and Cry6Aa represent two distinct families. The structure of Cry5Ba is similar to that of insecticidal 3d-Cry, and shows the conserved three-domain (3-d) architecture responsible for pore formation in insecticidal crystal proteins [20]. However, Cry6Aa does not show the typical 3-d architecture. In contrast to the insect model, the mode of action of nematicidal crystal toxins has been investigated only in *C. elegans* using the Cry5Ba [21]. As previously shown, the receptors for crystal protein Cry5Ba in *C. elegans* are invertebrate-specific glycolipids [21]. The Cry5Ba-resistant glycolipid mutants are sensitive to Cry6Aa [22]. The above information implies that the Cry6Aa may utilize a different toxicity pathway from Cry5Ba.

In *C. elegans*, necrotic cell death can be induced by extreme environmental stimuli or intrinsic insults, including hypoxia [23], ionic imbalance, heat stroke, bacterial infection, and

hypoosmotic shock [24]. In this study, we found that necrotic cell death can also be induced by *B. thuringiensis* crystal protein Cry6Aa. This pathway induced by Cry6Aa is mediated by aspartic protease (ASP-1). Additionally, ASP-1 protects the crystal protein Cry6Aa from over-degradation by *C. elegans*.

## Results

### ASP-1 is required for Cry6Aa-mediated toxicity

Proteomic approaches have previously been used to identify *B. thuringiensis* toxin binding proteins [25] and toxin receptors [26] and to understand insect resistance to *B. thuringiensis* [27]. Cry6Aa binding proteins in *C. elegans* were identified using 2-DE proteomics and ligand blotting. Separation of the *C. elegans* proteins by isoelectric focusing with a pH 4–7 IPG strip (18 cm) revealed that most proteins detected in 2-DE separations were smaller than 175 kDa and fell in the pH range of 4–6 (S1A Fig). Two-dimensional gel blots were probed with biotin-labeled Cry6Aa to identify *C. elegans* proteins that bound to Cry6Aa (S1B Fig). Fourteen silver-stained protein spots were detected (S1A Fig) and selected for identification. Four of these proteins were identified by mass spectrometry and peptide mass fingerprinting (PMF) (S1 Table), whereas the other spots were not identified. Spot 1 matched aspartic protease (ASP-1) from *C. elegans*, and Spots 2, 3 and 4 matched an ATP synthase subunit family member (ATP-2), actin and F58E2.4, respectively.

ASP-1 is mainly distributed in the intestinal cells of *C. elegans* [28]. The toxicity of crystal protein Cry6Aa toward *C. elegans* is believed to involve intestinal damage [29]. Therefore, ASP-1 is likely to be involved in Cry6Aa toxicity against *C. elegans*. To further characterize the interaction between ASP-1 and Cry6Aa, a ASP1-GST fusion protein was over-expressed in *Escherichia coli* (Fig 1A, lane 3) and was purified by affinity chromatography with glutathione Sepharose 4B (Fig 1A, lane 4). Ligand blot experiments showed that crystal protein Cry6Aa can bind to purified ASP1-GST fusion protein (Fig 1B, lane 6). In the control experiment, Cry6Aa did not bind to purified GST (Fig 1B, lane 7).

To facilitate the measurement of Cry6Aa toxin binding under non-denaturing conditions, purified ASP1-GST was dotted in increasing amounts on a membrane filter, and the filter was probed with biotin-labeled Cry6Aa. GST was a negative control, dot blot showed 3.2  $\mu$ g GST did not bind to Cry6Aa (Fig 1C). As the amount of dotted ASP1-GST protein increased, more biotin-labeled Cry6Aa was bound, and excess unlabeled Cry6Aa (1000-fold) competed for biotin-labeled Cry6Aa binding, which indicated that the binding between Cry6Aa and ASP1-GST was specific (Fig 1C). To measure the binding affinity of Cry6Aa to ASP1-GST, a competitive ELISA was performed. The dissociation constant (Kd) for ASP1-GST binding to Cry6Aa was 145.7 nM (126.8–164.7 nM) (Fig 1D). To assess whether ASP-1 and Cry6Aa interact directly, we determined the binding affinity between ASP-1 and Cry6Aa by isothermal titration calorimetry (Fig 1E). The estimated Kd was 126.4 nM (99.0–153.8 nM) (Fig 1E).

To test the role of Asp-1 *in vivo*, we compared the difference in larval growth inhibitory activities (GI) and mortality after treatment with Cry6Aa between wild type *C. elegans* N2 and mutant *asp-1* (*tm666*). For the quantitative growth test, the GI<sub>50</sub> values for N2 and *asp-1* (*tm666*) were  $4.9 \pm 0.6$   $\mu$ g/mL and  $45.1 \pm 3.7$   $\mu$ g/mL, respectively (S2 Table and Fig 2A). Their LC<sub>50</sub> values were  $63.7 \pm 6.8$   $\mu$ g/mL and  $715.6 \pm 69.3$   $\mu$ g/mL, respectively (S3 Table and Fig 2B). Lifespan measurements were performed in N2 and *asp-1*(*tm666*) upon exposure to Cry6Aa. As expected, the fraction of *asp-1*(*tm666*) alive was significantly higher than that of N2 (Fig 2C). The effects of different concentrations of Cry6Aa on the growth of L1 larvae of *C. elegans* N2 (top panels) and mutant *asp-1*(*tm666*) (middle panels) are summarized in Fig 2D. L1 larvae of N2 (Fig 2D, top panels) were not able to progress to adulthood after exposure to 30  $\mu$ g/mL

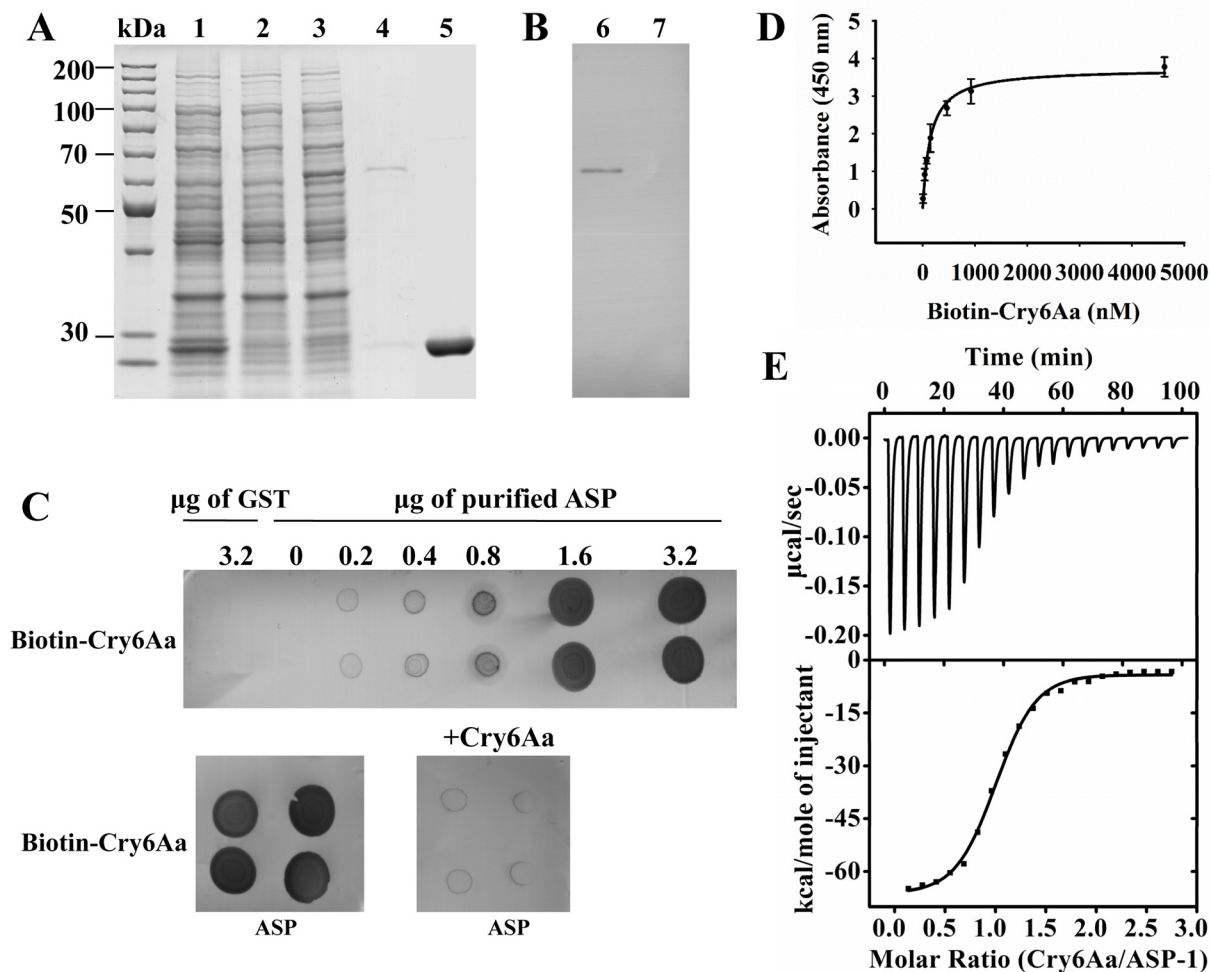


**Fig 1. The specific interactions between Cry6Aa and ASP-1.** (A) The expression and purification of ASP1-GST fusion protein in *E. coli*. Lane 1, *E. coli* BL21 containing pGEX-6p-1 vector with 0.1 mM IPTG induction under 16°C overnight, cell pellet; lane 2, *E. coli* BL21 containing pASP1-GST vector without IPTG induction, cell pellet. lane 3, *E. coli* BL21 containing pASP1-GST vector with 0.1 mM IPTG induction under 16°C overnight, cell pellet. lane 4, purified ASP1-GST fusion protein eluted from the glutathione Sepharose bulk; lane 5, purified GST tag eluted from the glutathione Sepharose bulk. (B) The binding of Cry6Aa to ASP1-GST fusion proteins by ligand blotting. The purified ASP1-GST fusion proteins (lane 6) or GST (lane 7) were separated by SDS-PAGE gels, and were transferred to a PVDF membrane. Filters were blocked overnight, and then probed with biotinylated Cry6Aa, Unbound toxin was removed by washing. The bound protein was detected streptavidin-horseradish peroxidase (HRP) conjugate. And finally the membrane was visualized. GST was the control. (C) ASP-1 proteins were dotted on a NC membrane directly and were probed with biotin labeled Cry6Aa or with biotin labeled Cry6Aa plus unlabeled Cry6Aa (1000-fold). GST was the control. (D) Binding affinity of Cry6Aa to ASP-1 was determined by ELISA. Ninety-six-well microtiter plates coated with ASP-1 were incubated with increasing concentrations of biotinylated Cry6Aa alone or with 1000-fold molar excess of unlabeled Cry6Aa to determine specific binding. Each point represents mean amounts of protein specifically bound. Specific binding was determined by subtracting nonspecific binding (with 1000-fold molar excess of unlabeled Cry6Aa) from total binding (without excess unlabeled Cry6Aa). (E) Isothermal titration calorimetric analysis of Cry6Aa binding to ASP-1. Titration of ASP-1 (2.20  $\mu\text{M}$ ) with 21.16  $\mu\text{M}$  Cry6Aa. The top panel show the raw data of the heat released, and the bottom panel show the binding isotherm fitted using nonlinear binding models. Data were analyzed in Origin 8.6 software after subtracting the heat released from titrating Cry6Aa alone into buffer. One of three representative experiments is shown.

doi:10.1371/journal.ppat.1005389.g001

Cry6Aa. However, the L1 larvae of mutant *asp-1(tm666)* (Fig 2D, middle panels) were able to progress to adulthood after the same exposure. These experiments indicated that the mutation of *asp-1* reduces the nematode's susceptibility to Cry6Aa.

When we transformed *asp-1(tm666)* with the whole *asp-1* gene, the rescued L1 larvae of *asp-1(tm666)* were unable to progress to adulthood after exposure to 30  $\mu\text{g}/\text{mL}$  Cry6Aa (Fig 2D, bottom panels, and Fig 2E), which indicates that the whole *asp-1* gene was sufficient to

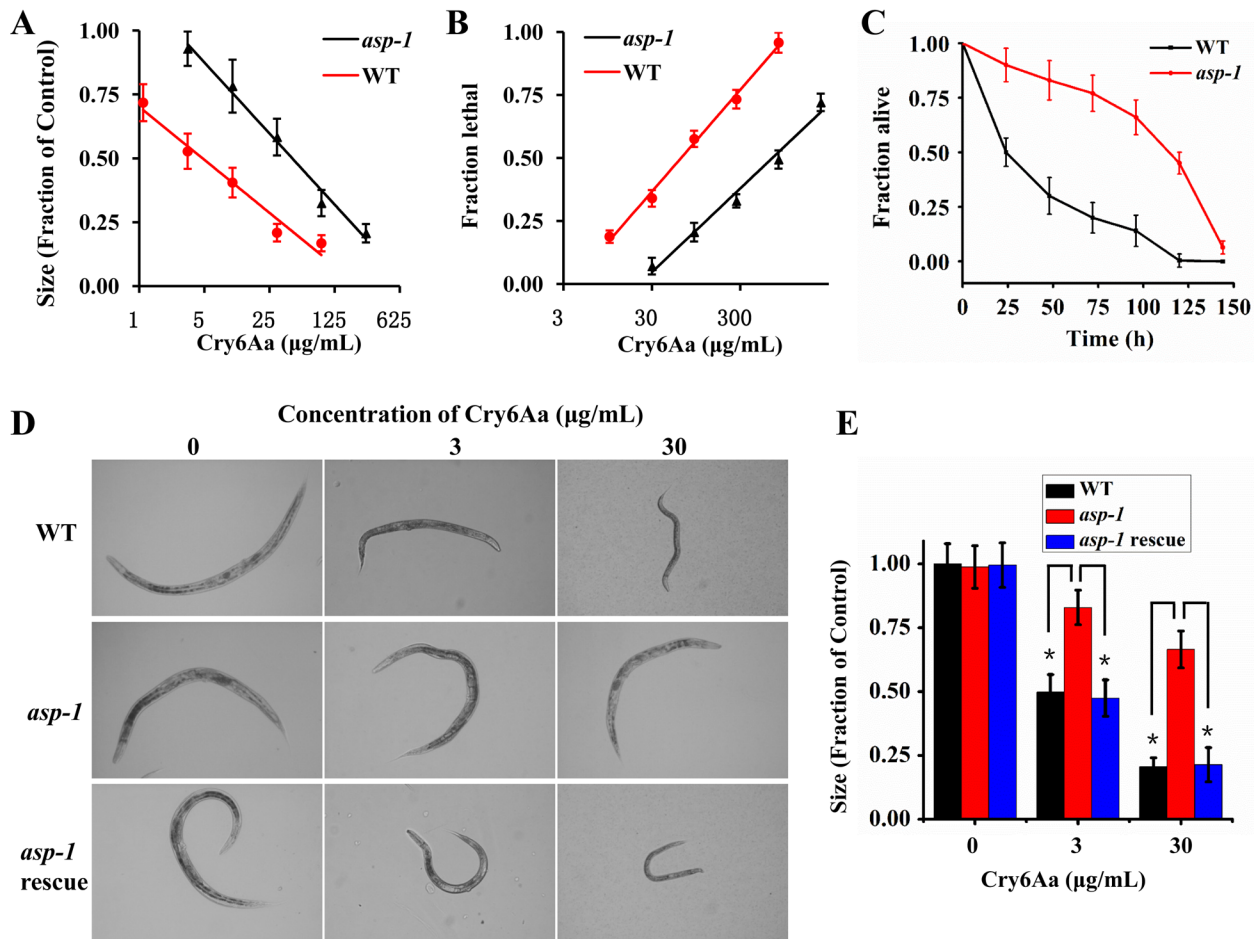


**Fig 2. The susceptibility of mutant *asp-1(tm666)* to Cry6Aa.** (A) Cry6Aa quantitative growth assay with wild type N2 and mutant *asp-1(tm666)*. (B) Cry6Aa lethality assay with N2 and *asp-1(tm666)*. The strains (as shown) were exposed to five doses of Cry6Aa. (C) Survival of wild type N2 and mutant *asp-1(tm666)* exposed to Cry6Aa. (D) Growth assay of different concentrations of Cry6Aa against L1 larvae of N2 (top panels), *asp-1(tm666)* (middle panels), and *asp-1(tm666)* rescued with the whole *asp-1* gene (bottom panels) observed under a light microscope. (E) Cry6Aa quantitative growth assay with N2, *asp-1(tm666)* and *asp-1(tm666)* transformed with the whole *asp-1* gene. Data were showed as mean  $\pm$  SD (n = 3).

doi:10.1371/journal.ppat.1005389.g002

restore susceptibility to Cry6Aa in the *asp-1(tm666)* mutant background. Taken together, these results indicate that ASP-1 is required for Cry6Aa-induced *C. elegans* death.

**ASP-1 mediated protection of Cry6Aa in *C. elegans*.** Bt protoxins are often activated to smaller active toxin, and insect midgut proteases are essential for the activation of Bt protoxins [30]. To monitor the size of Cry6Aa that is found inside the nematode, N2 and *asp-1(tm666)* were fed purified Cry6Aa proteins. Total proteins were then extracted from crystal protein treated nematodes, separated by SDS-PAGE, and subjected to Western blot analysis using an anti-Cry6Aa antibody. Only the fragment A2 (S2 Fig, arrow in black) is present in N2 background. However, in the *asp-1(tm666)* background, both fragment A2 (S2 Fig, black arrow) and fragment A3 (S2 Fig, blue arrow) coexist.

When Cry6Aa protoxin (S3A Fig, band A1, arrow in red) was digested by crude protein extracts from *C. elegans* N2 and *asp-1(tm666)*, only the fragment A2 (S3A Fig, arrow in black) is present in N2 background. However, in the *asp-1(tm666)* background, both fragment A2 (S3A Fig, black arrow) and fragment A3 (S3A Fig, blue arrow) coexist. A bioassay showed that the activities of the *asp-1(tm666)* digested fragments were reduced compared with that of the

full-length Cry6Aa toxin and the N2 digested fragments (S3B Fig). Therefore, fragment A2 (S3A Fig, black arrow) corresponds to the active toxin, and the over-degradation fragment A3 (S3A Fig, blue arrow) corresponds to the inactive toxin, which suggests that one of the roles of ASP-1 is to protect Cry6Aa against gut proteases.

To further demonstrate the protective effect of ASP-1, we pre-incubated Cry6Aa with ASP-1 and then exposed it to the extract from *asp-1* mutant worms and found that the misprocessed fragment disappeared (S3A Fig). This protective process restored the toxicity of the pre-incubated Cry6Aa to N2 (S3B Fig). These results provide additional support for the idea that ASP-1 mediates the protection and stabilization of Cry6Aa.

**Cry6Aa triggers the necrosis pathway in *C. elegans*.** Apoptosis and necrosis are the two major modes of cell death [1]. Propidium iodide (PI), which is a nucleic acid stain, acts as a marker for plasma membrane integrity, as it is only able to permeate cells when membrane integrity is disrupted, such as cells occur in necrosis [31,32]. Thus, PI can be used to distinguish between apoptotic cells and necrotic cells [31]. It is reported that propidium iodide is used as a marker of necrotic cell death [33,34]. When nematodes were exposed to Cry6Aa, intestinal cells of wild type nematode lost membrane integrity as shown by uptake of propidium iodide (Fig 3). However, the uptake of propidium iodide was significantly suppressed in nematode treated with necrosis inhibitors (Fig 3) or in some necrosis mutants (S4 and S5 Figs). Thus, we hypothesized that Cry6Aa might trigger necrotic cell death in the nematode.

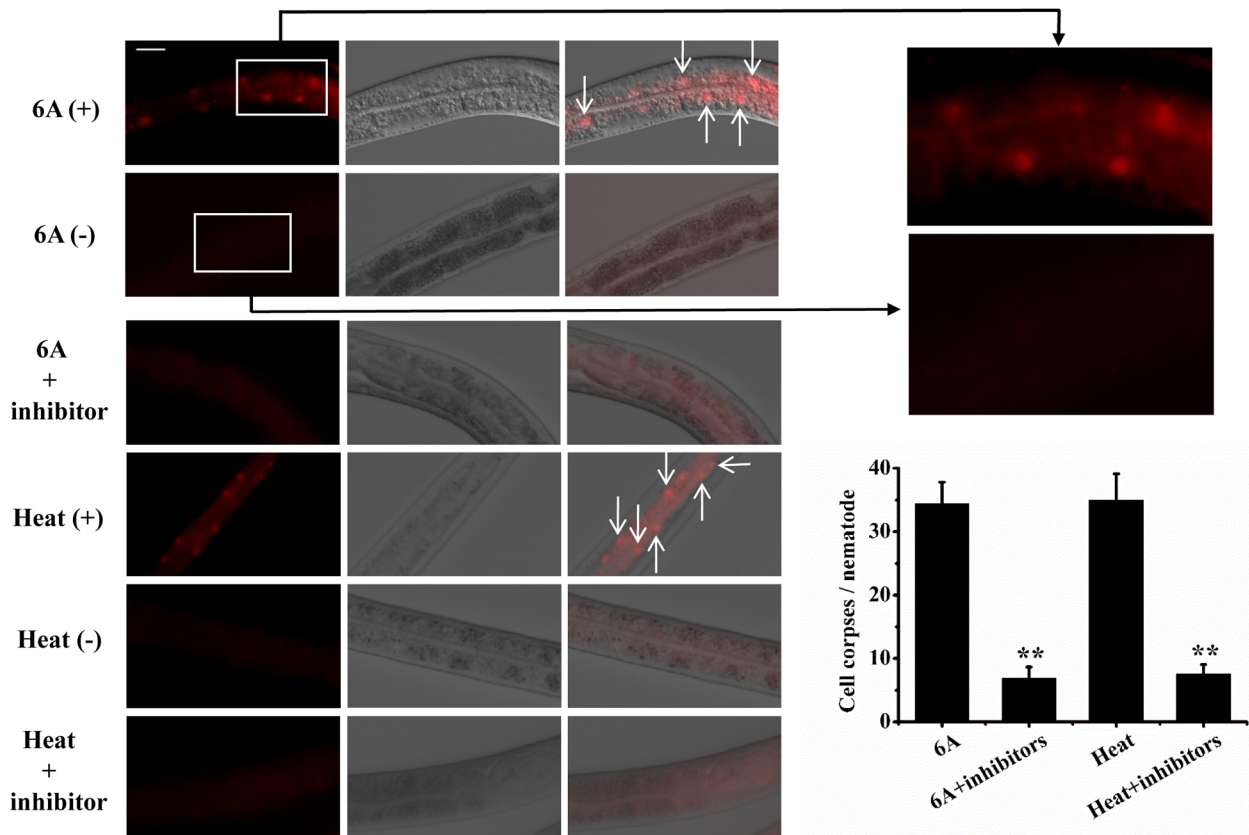


**Fig 3. Intestinal cell plasma membrane integrity was lost in wild type nematode N2 after exposure to Cry6Aa or heat stroke.** Heat stroke was a positive control. Fluorescence microscopy was used to monitor propidium iodide uptake. Arrows indicate intestinal cells stained with propidium iodide due to loss of membrane integrity. Two of the fluorescent images were magnified (boxed inset). The numbers of cell corpses per nematode were counted (Right). These results are the mean ± SD of three independent experiments. Double asterisks indicate  $p < 0.01$ . The bar denotes 20  $\mu\text{m}$ .

doi:10.1371/journal.ppat.1005389.g003

It is reported that heat stroke triggered extensive necrotic cell death in *C. elegans* [35,36]. Therefore, heat stroke is used as a positive control in this study. As expected, when nematodes were exposed to heat stroke, intestinal cells of nematode lost membrane integrity as shown by uptake of propidium iodide (Fig 3). However, the uptake of propidium iodide was significantly suppressed in nematode treated with necrosis inhibitors (Fig 3).

Necrosis is characterized by the rupture of lysosomes [37,38]. We examined whether Cry6Aa induces intestinal cell lysosomal rupture. First, *in vitro*, the intestinal lysosomal marker lysotracker was used to examine the lysosomal integrity during Cry6Aa-induced death. As expected, killing with Cry6Aa (Fig 4A) or heat stroke (Fig 5A) resulted in a burst of red fluorescence, indicating gut granule lysis. Second, *in vivo*, a *C. elegans* transgenic (pw1s50) strain expressing the intestinal lysosomal marker LMP-1::GFP [39,40] was used to examine lysosome integrity. GFP-labeled lysosome was found to be diffused upon treatment with Cry6Aa (Fig 4B) or heat stroke (Fig 5B). However, the gut granule lysis was significantly suppressed in

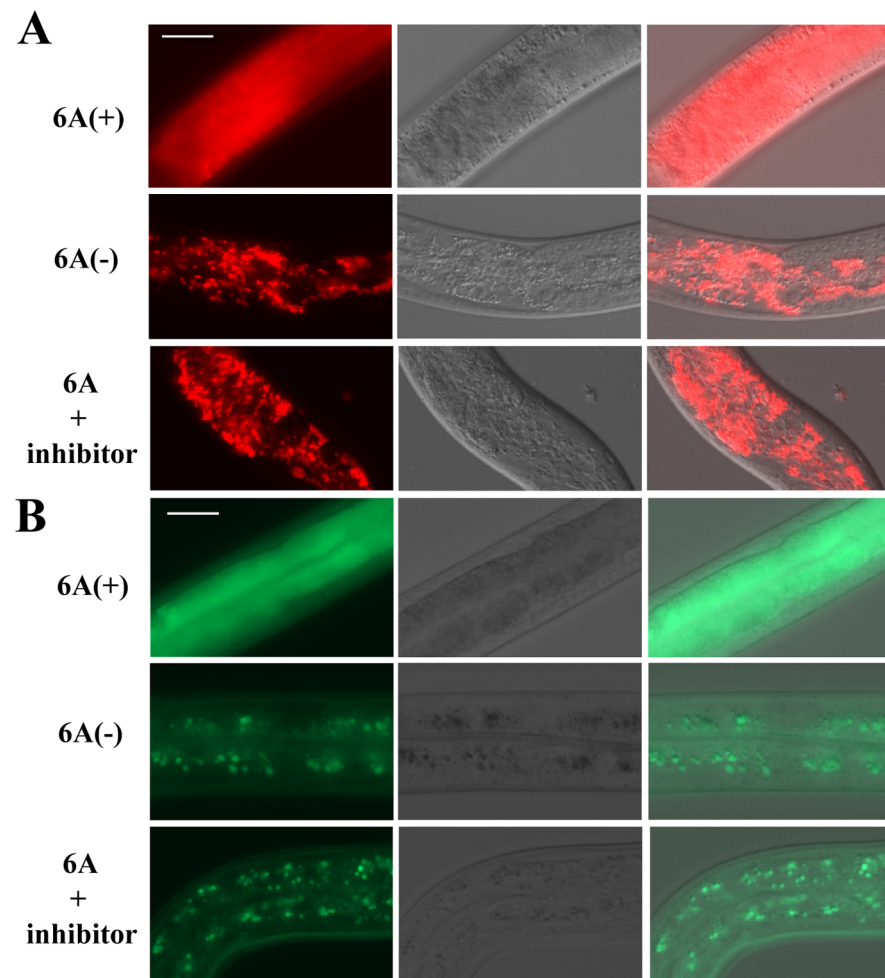


**Fig 4. Cry6Aa-induced intestinal cell lysosomal rupture in *C. elegans*.** (A) DIC and fluorescence microscopy of nematodes labeled with the intestinal lysosomal marker LysoTracker. (B) DIC and fluorescence microscopy of nematode RT258 (LMP-1::GFP strain). The intestinal lysosomal marker LMP-1::GFP was used to examine lysosomal integrity. The controls without Cry6A show significant staining, indicating that fluorescent gut lysosomes remained intact. In the Cry6A treated nematode, the labeled lysosome was found to be diffused (Fig 4A), indicating that Cry6Aa induces intestinal cell lysosomal rupture.

doi:10.1371/journal.ppat.1005389.g004

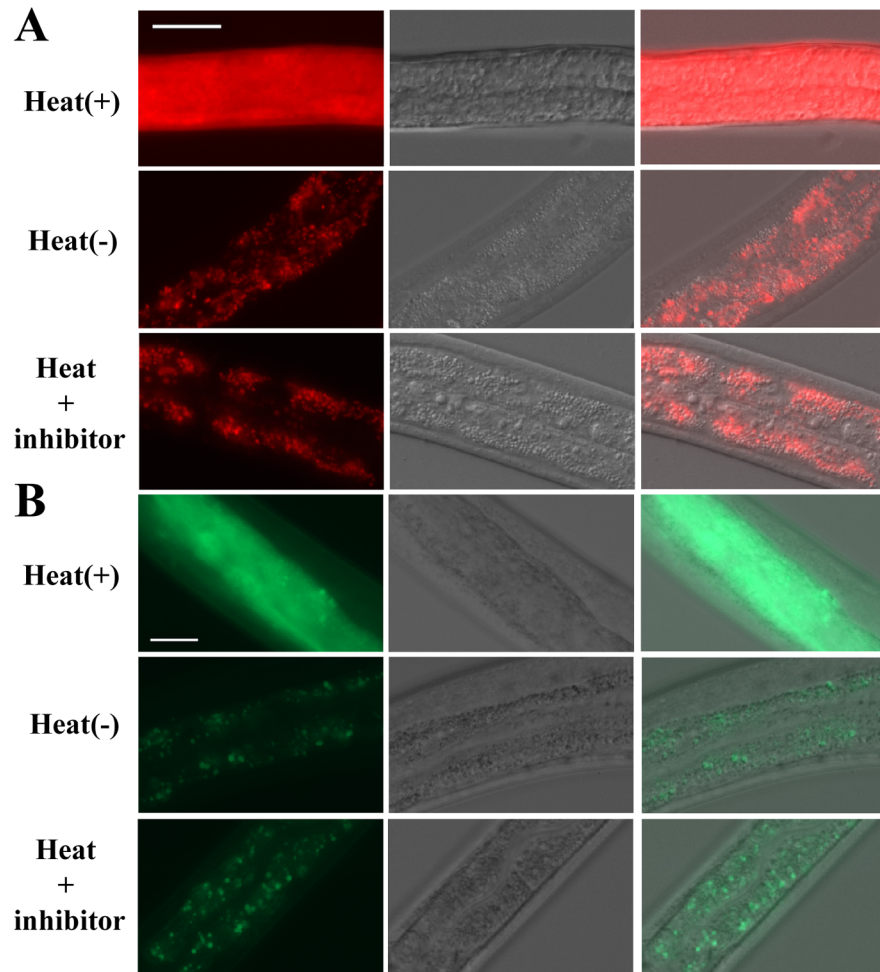


**Fig 5. Heat stroke induced intestinal cell lysosomal rupture in *C. elegans*.** (A) DIC and fluorescence microscopy of nematodes labeled with the intestinal lysosomal marker LysoTracker. (B) DIC and fluorescence microscopy of nematode RT258 (LMP-1::GFP strain). The intestinal lysosomal marker LMP-1::GFP was used to examine lysosomal integrity. In the nematode without heat stroke, fluorescent gut lysosomes remained intact. In the heat stroke treated nematode, the loss of lysosomal membrane integrity was accompanied by diffused fluorescence.

doi:10.1371/journal.ppat.1005389.g005

nematode treated with a necrosis inhibitor (Figs 4 and 5). These *in vivo* and *in vitro* experiments indicated that Cry6Aa induces intestinal cell lysosomal rupture.

An increase in the concentration of cytoplasmic calcium ( $[Ca^{2+}]_i$ ) is required for activation of necrosis [41]. We examined whether Cry6Aa affects concentration of cytoplasmic calcium. First, *in vitro*, changes in  $[Ca^{2+}]_i$  can be assessed by measuring cytoplasmic fluorescence using the calcium indicator Fluo-4 AM [36]. As expected, killing with Cry6Aa resulted in an increase in fluorescence of 1.5-fold (Fig 6A), which indicated an increase in  $[Ca^{2+}]_i$ . Second, *in vivo*, a *C. elegans* strain carrying an integrated transgene (rnyEx109) that expresses the calcium indicator d3cpv under the control of the intestine-limited promoter Pnhx-2 was used to monitor intracellular  $Ca^{2+}$  concentrations by fluorescence-resonance energy transfer (FRET) assay [42,43]. In this study, the relative cytosolic  $Ca^{2+}$  concentration is showed as the FRET ratio (defined as the fluorescence intensity in the FRET channel divided by the intensity in the CFP channel) [41,42]. The FRET ratio of controls without Cry6A was 0.64, indicating low levels of calcium.

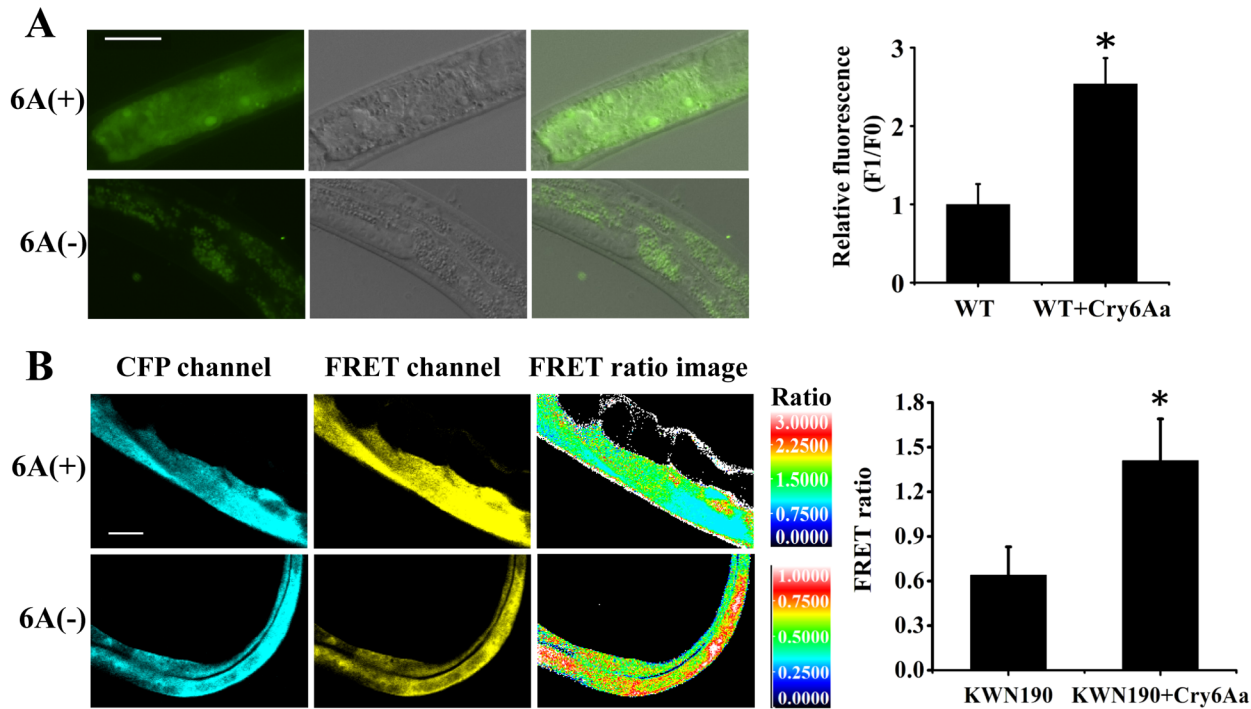


**Fig 6. Cry6Aa-induced an increase in cytoplasm calcium concentration in *C. elegans*.** (A) The rise in  $[Ca^{2+}]_i$  in the intestine of wild type nematode N2 induced by 63  $\mu\text{g}/\text{mL}$  Cry6Aa for 6 days. Fluorescence microscopy was used to monitor calcium concentration by measuring cytoplasmic fluorescence using the calcium indicator Fluo-4 AM. The right part shows the quantification of the fluorescence levels. These results are the mean  $\pm$  SD of three independent experiments. A single asterisk indicates  $p < 0.05$ . The bar denotes 20  $\mu\text{m}$ . (B) Representative CFP, FRET and Ratio images in transgenic nematode KWN190 upon exposure to 63  $\mu\text{g}/\text{mL}$  Cry6Aa for 6 days. Calcium levels were visualized using the calcium indicator d3cpv expressed from the intestine-limited promoter in KWN190. Right shows that the FRET ratio increased upon exposure to Cry6Aa. The image is representative of three independent experiments. A single asterisk indicates  $p < 0.05$ . The bar denotes 20  $\mu\text{m}$ .

doi:10.1371/journal.ppat.1005389.g006

The FRET ratio with Cry6Aa was 1.41, indicating high levels of calcium. We observed a 120% increase in the FRET ratio upon exposure to Cry6Aa (Fig 6B), which indicated an increase in  $[Ca^{2+}]_i$ . These *in vivo* and *in vitro* experiments indicated that Cry6Aa induced an increase in cytoplasm calcium concentration.

At the organismal level, it is reported that necrotic death is accompanied by a burst of intense death fluorescence (DF) after the worms respond to the necrosis inducing stimuli [43]. As expected, both of heat stroke (S6 Fig) and Cry6Aa (S7A Fig) led to a burst of death fluorescence.

Taken together, the above results support the idea that Cry6Aa triggers the necrosis pathway in *C. elegans*.

### A deficiency in the necrosis pathway confers tolerance to Cry6Aa

Necrosis in *C. elegans* requires an increase in intracellular  $Ca^{2+}$  levels mediated by the inositol triphosphate receptor ion channel (ITR-1), the calcium-dependent cysteine protease mediated by calpain TRA-3, lysosomal lysis for cytosolic acidification mediated by the vacuolar proton translocating ATPase (VHA-12), and the destructive release of lysosomal killer cathepsin proteases mediated by ASP-3 [44] or ASP-4 [43,44].

To examine whether necrosis is implicated in host defenses or for disease susceptibility during Cry6Aa targeting nematode, we compared the difference in mortality after treatment with Cry6Aa between wild type *C. elegans* N2 and necrosis mutants. Relative to the wild type,

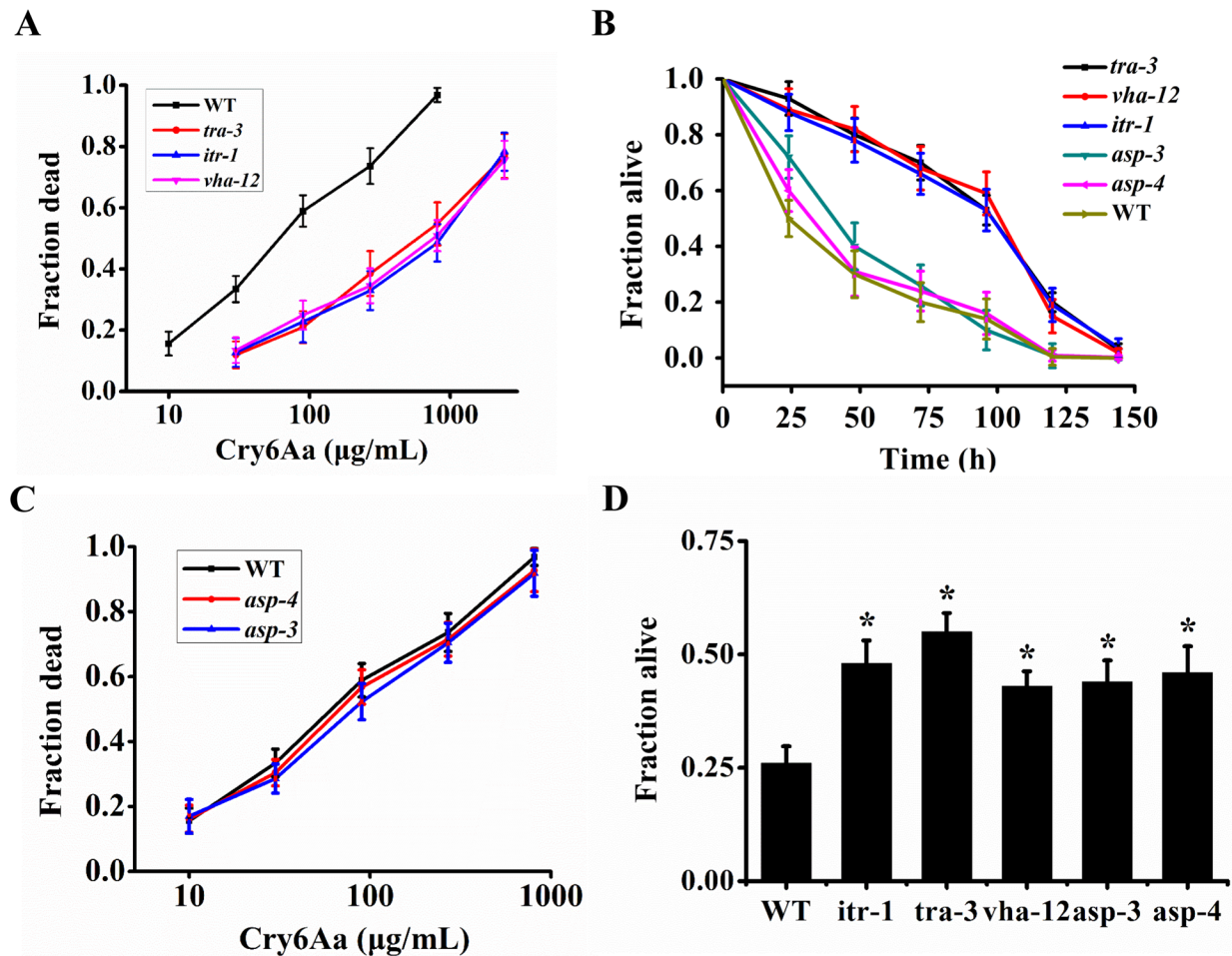


**Fig 7. The susceptibility of necrosis mutants to Cry6Aa.** (A) Cry6Aa lethality assay with *itr-1(sa73)*, *tra-3(e1107)*, and *vha-12(ok821)* necrosis mutants. The strains (as shown) were exposed to five doses of Cry6Aa. (B) Survival of *itr-1(sa73)*, *tra-3(e1107)*, *vha-12(ok821)*, *asp-3(tm4559)*, and *asp-4(ok2693)* necrosis mutants exposed to Cry6Aa. Mutations in *itr-1(sa73)*, *tra-3(e1107)*, and *vha-12(ok821)* reduced the sensitivity of nematodes to Cry6Aa. (C) Cry6Aa lethality assay with *asp-3(tm4559)* and *asp-4(ok2693)*. The strains (as shown) were exposed to five doses of Cry6Aa. (D) Survival of *itr-1(sa73)*, *tra-3(e1107)*, *vha-12(ok821)*, *asp-3(tm4559)*, and *asp-4(ok2693)* necrosis mutants exposed to heat stroke. Mutations in *itr-1(sa73)*, *tra-3(e1107)*, and *vha-12(ok821)* reduced the sensitivity of nematodes to heat stroke. A single asterisk indicates  $p < 0.05$ . Data were showed as mean  $\pm$  SD ( $n = 3$ ).

doi:10.1371/journal.ppat.1005389.g007

mutations in *itr-1(sa73)*, *tra-3(e1107)*, and *vha-12(ok821)* reduced the sensitivity of nematodes to Cry6Aa since their  $LC_{50}$  values were  $614.9 \pm 70.6$   $\mu$ g/mL,  $539.8 \pm 81.4$  and  $594.2 \pm 68.5$   $\mu$ g/mL, respectively (S3 Table and Fig 7A). Lifespan measurements were performed in N2 and these mutations upon exposure to Cry6Aa. As expected, the fraction of *itr-1(sa73)*, *tra-3(e1107)*, and *vha-12(ok821)* alive was significantly higher than that of N2 (Fig 7B). These experiments indicated that these mutations are tolerant to the crystal protein Cry6Aa. However, neither the necrosis mutant *asp-3(tm4559)* nor *asp-4(ok2693)* significantly suppressed the induction of nematode death by Cry6Aa (S3 Table and Fig 7C). Heat stroke was a positive control, as expected, relative to the wild type, mutations in *itr-1(sa73)*, *tra-3(e1107)*, *vha-12(ok821)*, *asp-3(tm4559)* and *asp-4(ok2693)* reduced the sensitivity of nematodes to heat stroke (Fig 7D).

Taken together, these results indicate that a deficiency in the necrosis pathway confers tolerance to Cry6Aa.

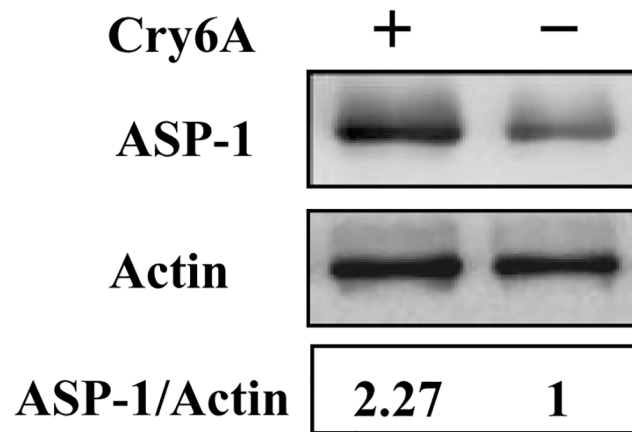


**Fig 8. The protein expression of *asp-1* was up regulated in *C. elegans* upon exposure to Cry6Aa.** Western blot shows the increased ASP-1 protein levels in *C. elegans* upon exposure to Cry6Aa. The blot is one of the three independent experiments.

doi:10.1371/journal.ppat.1005389.g008

**ASP-1 is required for Cry6Aa-induced *C. elegans* necrosis.** It has been reported that necrosis requires the killer cathepsin lysosomal proteases to dismantle the cell [44]. ASP-1 is a typical cathepsin lysosomal protease [44], and the above results confirmed that *asp-1* is required for Cry6Aa-mediated toxicity (Fig 2). Western blotting showed a 127% increase in the ratio of ASP-1/Actin upon exposure to Cry6Aa, which indicated that the protein expression of *asp-1* was up regulated in *C. elegans* upon exposure to Cry6Aa (Fig 8). To determine whether *asp-1* is required for Cry6Aa-induced *C. elegans* necrosis, propidium iodide staining was performed in Cry6Aa treatment of the mutant *asp-1(tm666)*. As expected, the uptake of propidium iodide was significantly suppressed in *asp-1(tm666)* upon exposure to Cry6Aa (S7B Fig). In addition, *asp-1(tm666)* was able to reduce death fluorescence induced by Cry6Aa (S7A Fig). Examination of the intestinal lysosomal marker lysotracker showed that the burst of red fluorescence was significantly suppressed in *asp-1(tm666)* upon exposure to Cry6Aa (S7C Fig), indicating that *asp-1* is required for Cry6Aa-induced intestinal lysosomal rupture.

Together, these results suggest that the Cry6Aa-induced necrosis pathway is mediated by ASP-1.

**The necrosis pathway is specifically induced by Cry6Aa, not by Cry5Ba.** To determine whether the mutant *asp-1(tm666)* was specifically tolerant to Cry6Aa or to nematocidal crystal proteins in general, we tested *asp-1(tm666)* for tolerance to another nematocidal crystal protein, Cry5Ba. Both mutant *asp-1(tm666)* and the wild-type N2 were sensitive to Cry5Ba at the same level (Fig 9A and 9B). In addition, none of the necrosis mutants suppressed Cry5Ba-induced death in *C. elegans* (Fig 9C).

To test whether Cry5Ba can bind to ASP-1, purified Cry5Ba and Cry6Aa was dotted on a membrane filter, and the filter was probed with biotin-labeled ASP-1. Cry6Aa was a positive control, and dot blot showed Cry5Ba did not bind to ASP-1 (Fig 10A). Ninety-six-well microtiter plates coated with ASP-1 were incubated with increasing concentrations of biotinylated Cry5Ba. ELISA showed Cry5Ba did not bind to ASP-1 (Fig 10B). These results indicate that Cry5Ba is not able to bind to ASP-1.

Calcium concentration can be assessed by measuring cytoplasmic fluorescence using the calcium indicator Fluo-4 AM [36]. Heat stroke was a positive control, as expected, heat stroke induced an increase in cytoplasm calcium concentration. However, killing with Cry5Ba did not affect intracellular calcium concentration (S8 Fig).

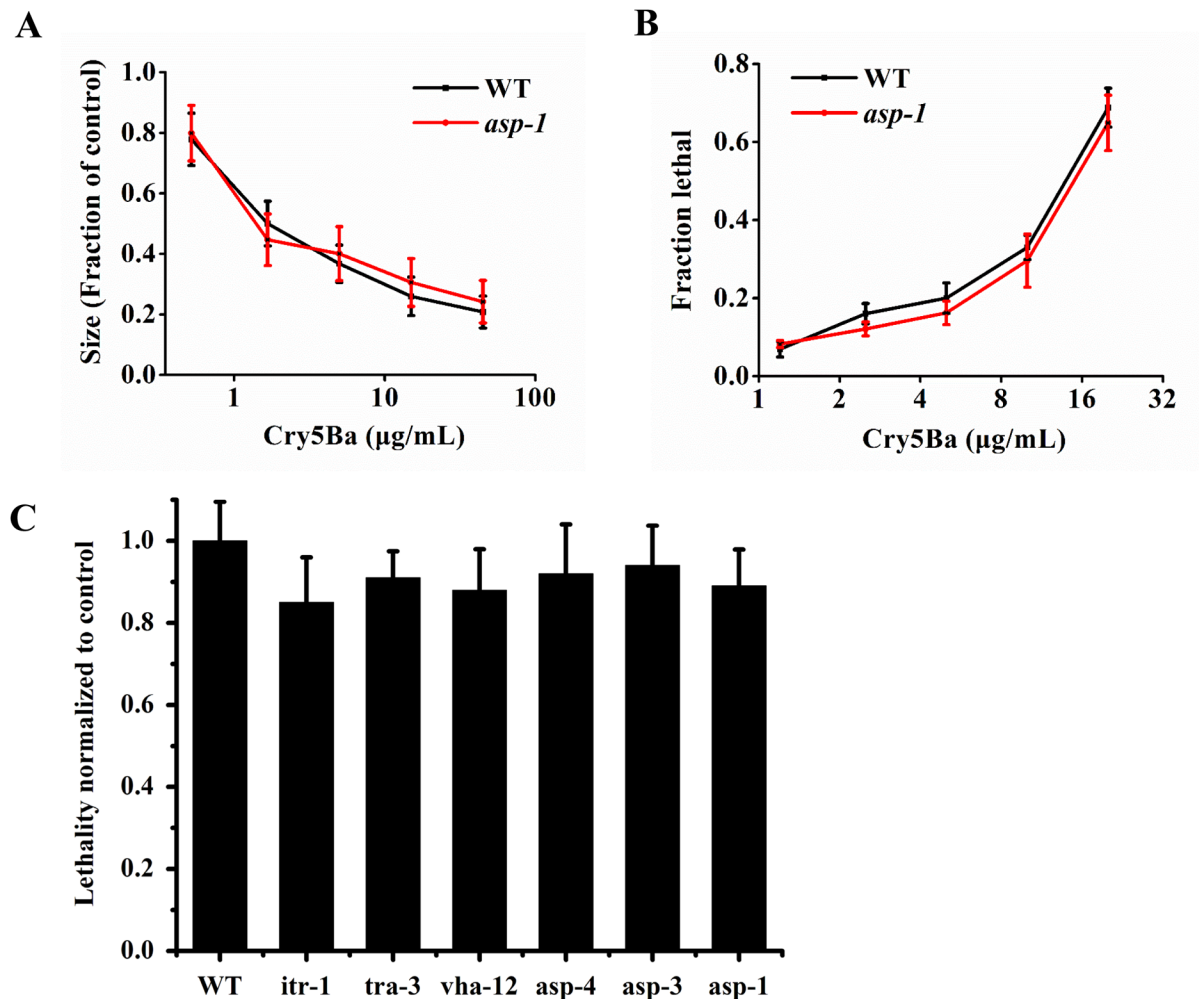


**Fig 9. The susceptibility of necrosis mutants to Cry5Ba.** (A) Cry5Ba quantitative growth assay with wild type N2 and mutant *asp-1(tm666)*. (B) Cry5Ba lethality assay with N2 and *asp-1(tm666)*. The strains (as shown) were exposed to five doses of Cry6Aa. (C) Lethality of necrosis mutants exposed to Cry5Ba. Data were showed as mean  $\pm$  SD (n = 3).

doi:10.1371/journal.ppat.1005389.g009

Together, these results indicate that the necrosis pathway is specifically induced by Cry6Aa, not by Cry5Ba.

## Discussion

The classical, pore-forming model is the widely accepted model for describing the mode of action of 3d-Cry. This model elucidates crystal protein action at the biochemical level, which includes crystal protein activation, receptor binding, pore formation, and cell lysis [10–13]. The identified receptors in the pore-forming model, such as cadherin, aminopeptidase (APN), and alkaline phosphatase (ALP), mediate insect resistance to 3d-Cry [45]. However, these receptors were not identified in *C. elegans* by the Cry6Aa-ligand blotting assay. These results indicate that the mode of action of non-3d crystal protein Cry6Aa against *C. elegans* may be different from the classical pore-forming model. The signal transduction model proposed that crystal proteins activate a Mg<sup>2+</sup>-dependent adenylyl cyclase (AC)/protein kinase A (PKA) signaling pathway [14,15]. This work show that crystal protein Cry6Aa triggers the Ca<sup>2+</sup>-dependent calpain–cathepsin necrosis pathway in *C. elegans*. Thus, in contrast to the classical pore-

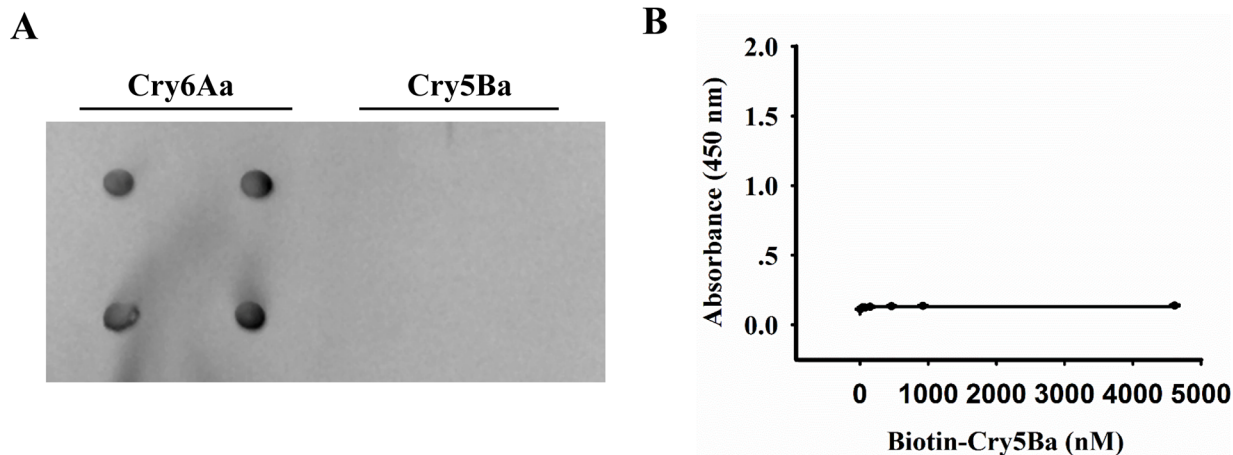


**Fig 10. Cry5Ba is not able to bind to ASP-1.** (A) Purified Cry5Ba and Cry6Aa were dotted on a NC membrane directly and were probed with biotin labeled ASP-1. Cry6Aa was the positive control. (B) Binding affinity of Cry5Ba to ASP-1 was determined by ELISA. Ninety-six-well microtiter plates coated with ASP-1 were incubated with increasing concentrations of biotinylated Cry5Ba.

doi:10.1371/journal.ppat.1005389.g010

forming model, which elucidated at the biochemical level, the present findings reveal that crystal toxin triggers cell death by necrosis signaling pathway. This is the first demonstration that deficiency in necrosis pathway confers tolerance to Bt crystal protein.

Apoptosis occurs in embryonic and larval development. The CED-3 caspase, which is regulated by pro-apoptotic (CED-4, EGL-1) and anti-apoptotic (CED-9) factors, is involved in apoptosis [36,46]. However, we found that neither *ced-3* (*n171*), *ced-4* (*n1162*), nor *ced-9* (*1950*) mutation changed Cry6Aa-induced death (S9 Fig). Therefore, cell death induced by Cry6Aa does not depend on the apoptotic machinery.

Autophagy is required for necrosis induced by prolonged hypoxia in *C. elegans* [47]. Conversely, autophagy protects *C. elegans* against necrosis during *Pseudomonas aeruginosa* infection [48]. *Lgg-1* encodes the *C. elegans* ortholog of Atg8/LC3 that facilitates autophagic vesicle growth, and *lgg-1* is involved for autophagy [38,49]. *Unc-51* encodes the serine threonine kinase ortholog of yeast autophagy protein Atg1 [50]. However, we found that neither *unc-51* (*e1189*) nor *lgg-1* (*bp500*) mutations suppressed or promoted Cry6Aa-induced death (S10 Fig). The above information suggest that autophagy plays different role respond to different pathological conditions.

An increasing number of bacterial pathogens have been shown to induce necrosis in host cells [2]. For example, *Erwinia carotovora*, *Photobacterium luminescens*, and *Enterococcus faecalis* are reported to induce necrosis in *C. elegans* [51].  $\beta$ -Toxin from *Clostridium perfringens*, alpha-toxin from *Clostridium septicum*, and *Helicobacter pylori* VacA [2] are reported to cause necrosis. Our study reveals that *B. thuringiensis* toxin triggers necrosis pathway in *C. elegans*. That Cry6A triggers necrosis represents a newly added necrosis paradigm in the *C. elegans*. Our findings contribute to the understanding of the mechanisms of host-pathogen interactions in higher species.

Necrosis plays an important role in host-pathogen interactions which can be used by both sides [2]. In some cases, necrosis plays a significant role in antiviral/antibacterial host defense [2,8]. For example, herpes simplex virus 1 (HSV-1) protein is reported to trigger an effective host-defense mechanism by activating RIP3/MLKL-dependent necrosis [52]. In others, necrosis does not as a host defense, but as pathogen survival strategy to aid its spread [2]. For example, cIAP2-dependent antagonism of RIPK3-mediated programmed necrosis critically protects the host from influenza infection [53]. Besides, it is reported that *E. carotovora* and *P.*

*luminescens* used the necrosis to develop their effective virulence [51]. Our study reveals that deficiency in necrosis pathway confers tolerance to Bt crystal protein. It is possible that necrosis plays different role respond to different pathogens or toxins.

In the present work, evidence is presented that Bt crystal protein Cry6Aa triggers the necrosis pathway in *C. elegans* mediated by ASP-1, not by ASP-4 or ASP-3. To test whether ASP-1 is specifically required for Cry6A-induced necrosis, the *asp-1(tm666)* nematodes are exposed to two other death-inducing stimuli, heat stroke and hypoxia. We found that both mutant *asp-1(tm666)* and the wild-type N2 were sensitive to either heat stroke or hypoxia at the same level (S11 Fig). Thus, there is some difference in the necrosis pathway induced by Cry6Aa compared to other stressors, and ASP-1 is specifically required for Cry6A-induced necrosis. Previous studies of the cellular necrosis pathway have largely focused on neurodegeneration [43], where intrinsic insults induce necrosis mediated by ASP-3 and ASP-4 [44]. Recently, this pathway in the nematode intestine was reported, where lethal stress induced necrosis in *C. elegans* mediated by ASP-4 [43]. We recently found a two-domain protein named Nel, which is composed of a necrosis-inducing phytophthora protein 1-like domain found in phytopathogens and a ricin B-like lectin domain, induced necrosis mediated by ASP-4 [54]. Therefore, we speculate that different aspartyl proteases in the necrosis pathway respond to different death-inducing stimuli.

Our study show that Cry6A binds to ASP-1 and that ASP-1 mediates the protection and stabilization of Cry6Aa. This stabilization effect could be similar to that cadherin-mediated protection of Cry1Fa toxin from protease degradation in the insect gut [55]. ASP-1 is mainly distributed in the intestinal cells of *C. elegans* [28]. To explain how an intracellular ASP-1 protein binds Cry6Aa, we fed rhodamine labeled Cry6A to *C. elegans*, and monitored the signal of rhodamine-labeled crystal proteins with confocal microscope. As expected, the labeled Cry6A toxin was internalized into intestinal cells (S12 Fig).

A phylogenetic tree of the aspartyl proteases were constructed. ASP-1 from *C. elegans* belongs to the nematode-specific aspartyl protease class; however, ASP-3 and ASP-4 from *C. elegans* belong to a distinct branch that also includes mammalian proteases [44]. These results provide a plausible explanation for the lack of toxicity of Cry6Aa toward mammals. We hypothesize that the Bt non-three-domain Cry6Aa evolved to recognize the nematode specific ASP-1 and thus to target nematodes.

Griffitts *et al.* reported that *C. elegans* glycolipid mutants with resistance to Cry5Ba were not resistant to Cry6Aa [22]. In the present study, the *C. elegans* necrosis mutants with tolerant to Cry6Aa, were not tolerant to Cry5Ba. The above observations indicate that pathway of Cry6Aa against nematodes is different from that of Cry5Ba. A possible explanation for this difference is that the sequence and structure of the Cry6Aa toxin are different from those of Cry5Ba. The structure of Cry5Ba is similar to that of insecticidal 3d-Cry, and shows the typical conserved three-domain (3-d) architecture responsible for pore formation in insecticidal crystal proteins [20]. However, the amino acid sequence of Cry6Aa is completely different from that of 3d-Cry, and Cry6Aa does not show the typical 3-d architecture. Accordingly, further research is necessary to determine the structure of Cry6Aa.

Both *B. thuringiensis* and nematodes coexist in the soil ecosystem. We recently reported that nematodes are an alternative dominant host that contributes to the persistence, growth, and transmission of *B. thuringiensis* [56]. Some strains of *B. thuringiensis* have evolved to become nematode pathogens and use the host to reproduce, other non-nematicidal strains can reproduce on nematodes killed by other means or can still use nematodes as a means to reach their true host [56]. Bt has evolved crystal proteins to help it reproduction inside the host nematode [29]. On the other hand, *C. elegans* has evolved some conserved pathways to protect against *B. thuringiensis* crystal proteins [57,58]. Our study reveals that *B. thuringiensis* toxin

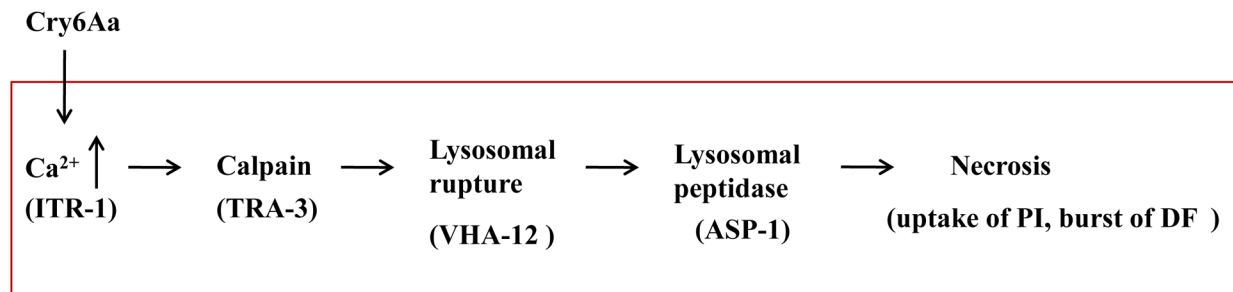


**Fig 11. The working model of crystal protein Cry6Aa.** Cry6Aa toxin triggers the Ca<sup>2+</sup>-dependent calpain–cathepsin necrosis pathway using Cry6Aa–*Caenorhabditis elegans* toxin–host interaction system, which involves an increase in concentrations of calcium, lysosomal lyses, the killer cathepsin proteases mediated by ASP-1, uptake of propidium iodide, and burst of death fluorescence. Abbreviations: PI, propidium iodide; DF, death fluorescence.

doi:10.1371/journal.ppat.1005389.g011

triggers cell death by the necrosis pathway. Therefore, our findings have potential implications for understanding the co-evolution between nematodes and *B. thuringiensis*.

In conclusion, the present study reveals that crystal toxin triggers the necrosis pathway using Cry6Aa–*C. elegans* toxin–host interaction system, which involves an increase in concentrations of calcium, lysosomal lyses, uptake of propidium iodide, and burst of death fluorescence (Fig 11). We show that aspartic protease ASP-1 is required for Cry6Aa induced necrosis, whereas intrinsic insults induce necrosis mediated by ASP-3 and ASP-4. Understanding this model could lead to new strategies for nematode control. Further research is necessary to establish the existence of additional steps in Cry6Aa action: for example, what is the functional receptor in the intestinal surface and the role of receptor in crystal toxin action? Identification of the receptor would provide new avenues for studying the nematicidal mechanisms of Cry6Aa.

## Materials and Methods

### *C. elegans* culture and strains

Maintenance of *C. elegans* strains was performed as previously described [59]. The mutated and transgenic strains used in this study include the following (S4 Table): *ced-3(n717)*, *ced-4(n1162)*, *ced-9(n1950)*, *itr-1(sa73)*, *tra-3(e1107)*, *vha-12(ok821)*, *asp-4(ok2693)*, *unc-51(e1189)*, *lgg-1(bp500)*, *pwIs50[lmp-1::GFP + Cbr-unc-119(+)]*, and *rnyEx109[nhx-2p::D3cpv + pha-1(+)]* were provided by the *Caenorhabditis* Genetics Center (<http://www.cbs.umn.edu/CGC/>). The *asp-3(tm4559)* and *asp-1(tm666)* (mutagen: TMP/UV) was obtained from Tokyo Women’s Medical College (<http://www.wormbase.org/db/gene/variation?name=tm666;class=Variation>). *C. elegans* was cultured using standard techniques, and the Bristol N2 strain was the wild type [59]. *RnyEx109* is an integrated transgene that directs expression of calcium indicator *d3cpv* under the control of intestine-limited promoter *Pnhx-2* [42,43]. *PwIs50* is an integrated transgene with the intestinal lysosomal marker *LMP-1::GFP* [39,40].

### Crystal protein purification and labeling

Cry6Aa and Cry5Ba proteins were purified according to our previously described method [60]. All purified protein samples were then solubilized in 20 mM HEPES (Calbiochem BB0364) (pH 8.0), quantified [61], and stored at -80°C. The purified Cry6Aa protein was labeled with N-hydroxysuccinimide-rhodamine (Pierce) or N-hydroxysulfosuccinimide ester-PC-biotin (Pierce), respectively, according to the manufacturer’s instructions.

## Nematode bioassays and lifespan analysis

The growth assay was performed according to the protocol described previously reported [62]. The LC<sub>50</sub> assay was performed according to the protocol reported by Marroquin *et al* [22]. All lifespan measurements were performed on NGM agar plates of *E. coli* express Cry6Aa at 20°C [48]. The lifespan was monitored at 24 h, 48 h, 72 h, 96 h, 120 h, 144 h. Nematodes that did not move when they were gently prodded and displayed no pharyngeal pumping were marked as dead [48].

## Two-dimensional electrophoresis (2-DE)

Preparation of the total protein of *C. elegans* was conducted according to the protocol described by Schrimpf *et al* [63]. 2-DE was performed according to the protocol described by Krishnamoorthy *et al* [25]. Strips of 18 cm (pH 4–7) in length were used. After 2-DE, Gels were either silver stained and scanned using a GS-800 calibrated densitometer (Bio-Rad), or transferred to polyvinylidene difluoride Q (PVDF) membrane filters (Immobilon P, Millipore) for ligand blotting.

## Ligand blotting

Ligand blotting was performed according to the protocol reported by Fernandez-Luna *et al* [26]. Total *C. elegans* proteins were separated by 2-DE, and gels were transferred to a PVDF membrane in transfer buffer (20% methanol, 25 mM Tris-base, 192 mM glycine) for 60 min. Filters were blocked overnight in PBST (0.1% Tween 20 in phosphate buffered saline, pH 7.4) containing 3% BSA. Blocked filters were incubated with biotinylated Cry6Aa (10 nM) for 2 h at room temperature, and then washed three times using PBST. The bound protein was detected by 1 µg/ml streptavidin-horseradish peroxidase (HRP) conjugate (Sigma, S5512). The membrane was visualized using enhanced chemiluminescence substrate (SuperSignal West Pico, Pierce) following the manufacturer's instructions.

## Western blotting

*C. elegans* treated with Cry6Aa were harvested and subsequently washed five times in M9 medium. Treated *C. elegans* samples were grinded with liquid nitrogen and were then subjected to sodium dodecyl sulfate polyacrylamide gel electrophoresis (SDS-PAGE) and transferred onto a PVDF membrane. Primary antibodies were anti-ASP-1 antibody (1:5000 dilution) for detection of ASP-1 expression. The secondary antibody was HRP-coupled anti-rabbit antibody (1:5000 dilution). The membrane was visualized as described above for the ligand blotting assay.

To monitor the size of Cry6Aa that is found inside the nematode, N2 and *asp-1(tm666)* were fed purified Cry6Aa proteins. Total proteins were then extracted from crystal protein treated nematodes, separated by SDS-PAGE, transferred onto a PVDF membrane. Primary antibodies were anti-Cry6Aa antibody (1:5000 dilution) for detection the size of Cry6Aa. The secondary antibody was HRP-coupled anti-rabbit antibody (1:5000 dilution). The membrane was visualized as described above for the ligand blotting assay.

## Dot blotting

Different quantities of ASP-1 were dotted onto a nitrocellulose (NC) membrane (Millipore, Bedford, MA, USA). After blocking with 3% bovine serum albumin (BSA) in PBST, NC membrane was bathed in biotinylated-Cry6Aa (10 nM) for 2 h at room temperature, washed three times using PBST. Unlabeled Cry6Aa (1000-fold excess) was used in the competition assays.

The bound protein was detected by 1 µg/ml streptavidin-horseradish peroxidase (HRP) conjugate (Sigma, S5512). Finally, the signal was visualized using 3, 3'-diaminobenzidine tetrahydrochloride (DAB) substrate (Pierce) following the manufacturer's instructions.

### Mass spectrometry

Selected spots were excised from the stained 2-DE gel and digested with trypsin, and the resulting peptide fragments were examined by mass spectrometry according to the method described by Krishnamoorthy *et al* [25]. Peptides were examined using matrix-assisted laser desorption ionization-time of flight mass spectrometry (MALDI-TOF-MS) system (4700 Proteomics Analyzer, Applied Biosystems). A database search of spectral data was conducted using a mascot search engine (Matrix Science) to search the *C. elegans* databases.

### Gene cloning, expression, and purification of aspartic protease (ASP-1) in *E. coli*

RNA was extracted from *C. elegans* using a total RNA isolation system (Promega, Madison, WI, USA). First strand cDNA was synthesized from total RNA according to the manual (Takara, Tokyo, Japan). The ASP-1 full-length coding gene was amplified from synthesized cDNA by polymerase chain reaction (PCR) using a pair of primers based on the sequences reported for the aspartic protease gene (GenBank NM\_171587): P1, 5'-CGCGAATTCATG CAGACCTTCGTTTT-3', *EcoRI* restriction site is underlined; P2, 5'-CTGCTCGAGCTTCAATCCCTTGTTGG-3', *XhoI* restriction site is underlined. The amplified fragments were purified, digested with *EcoRI* and *XhoI*, and cloned into vector pGEX-6P-1 to create a recombinant vector pASP1-GST. Then, plasmid pASP1-GST was transformed into *E. coli* strain BL21 (DE3) (Amersham Biosciences, Uppsala, Sweden), and positive transformants were selected on an LB plate containing 100 µg/ml ampicillin. The ASP-1 was overexpressed in *E. coli* as a GST-tagged fusion protein ASP1-GST. ASP1-GST was purified according to the GST bind kit protocol.

### *Asp-1* rescue assays

pPD49.26 was used as the vector backbone for test constructs. The rescuing fragment comprising the entire 2715 bp *asp-1* gene (GenBank AF210248) contains 1421 bp 5'-flanking DNA of *asp-1*, 1191 bp *asp-1* cDNA, and 103 bp 3'-UTR of *asp-1*. The 2.7 kb rescuing fragment was made by PCR amplification with *Pfu* polymerase using a pair of primers designed based on the sequences reported for the aspartic protease gene: P3, 5'-CGCGAATTC CAAAATGGGTCTTACC-3', *EcoRI* restriction site is underlined; P4, 5'-CTGCTCGAG ATCAGAAATTTAAAGATT-3', *XhoI* restriction site is underlined. The amplified fragment was purified, digested with *EcoRI* and *XhoI*, and cloned into vector pPD49.26 to create a recombinant vector pASP1RES. This construct was co-injected at 10 ng/ml with the dominant rol-6 marker (pRF4) at 50 ng/ml into the gonads of nematode *asp-1* (*tm666*) by standard techniques [64]. The eggs of roller hermaphrodites were allowed to hatch to obtain L1 larvae, and then the L1 larvae were treated with Cry6Aa. The nematode resistance to Cry6Aa was evaluated based on the ability of L1 larvae to progress to adulthood during the course of the experiment [65].

### Enzyme-linked immunosorbent assay (ELISA)

The purified Cry6Aa was biotinylated using *N*-hydroxysulfosuccinimide ester-PC-biotin (Pierce, Rockford, IL) according to the manufacturer's instructions. ELISA plates (high-binding, 96-well, Immulon 2HB; Thermo Fisher Scientific Inc., Waltham, MA) were incubated at

4°C for 12 h with 0.5 µg of ASP-1/well in 20 mM HEPES buffer (pH 8.0). The plates were then blocked at room temperature for 2 h in 100 µL PBST containing 3% BSA. For the binding assays, ELISA plates coated with ASP-1 were incubated with increasing concentrations of biotinylated Cry6Aa. For the competition assays, a 1000-fold molar excess of nonlabeled Cry6Aa was added to a solution that contained biotinylated Cry6Aa. Specific binding was determined by subtracting nonspecific binding (with 1000-fold molar excess of unlabeled Cry6Aa) from total binding (without excess unlabeled Cry6Aa). The other reaction conditions and the data analysis were conducted following the method described by Zhang et al [66]. Data were analyzed using SigmaPlot 12.0 software.

### Isothermal titration calorimetry (ITC)

Isothermal titration calorimetry experiments were performed at 25°C using the TAM Thermal Activity Monitor system (Thermometric AB, Sweden). Recombinant proteins ASP-1 were buffer-exchanged into 20 mM HEPES (pH 8.0) by G-25 spin-column chromatography. A solution containing 21.16 µM Cry6Aa in the same buffer was used as titrant, and solutions containing 2.20 µM ASP-1 were used in the calorimetry cell. The heat of reaction per injection was determined by integration of the peak areas using the Origin 8.6 software. ITC titration experiments were carried out with 20 injections, 10 µL per injection, and 75 s between each injection. Cry6Aa was titrated into 20 mM HEPES buffer to account for heat released due to dilution. Data were analyzed in Origin 8.6 software after subtracting the heat released from titrating Cry6Aa alone into buffer. The dissociation constants (Kd) were calculated from the plots of the total heat versus the molar ratio of Cry6Aa to ASP-1 [67].

### Proteolytic assays and protease protection assays

The experiments were based on the methodology of Frago *et al.* [68] with some modifications. Approximately 500 mg of N2 or *asp-1(tm666)* were triturated in 500 µL of acidic buffer (0.1 M sodium acetate and 0.5% v/v Triton-100; pH 4.8) at 4°C, centrifuged at 12,000g for 20 min, and the supernatant was used as crude protein extract. For proteolytic assays, 50 µL Cry6Aa was incubated with 50 µL crude protein extracts from wild type N2 or *asp-1(tm666)* for 2 h at 37°C. For protease protection assays, Cry6Aa was preincubated with ASP-1 or GST (control), and then treated with crude protein extracts from *asp-1(tm666)*. For the toxicity of the digested Cry6Aa, the sample buffer was replaced by HEPES buffer (pH 8.0), and the nematodes N2 were exposed to digested Cry6Aa for lifespan analysis.

### Death fluorescence (DF) measurements

Nematodes were imaged on a 2% agarose pad prepared on glass slides, and images were acquired using an Olympus BX63 microscope. Death fluorescence was observed through a DAPI filter ( $\lambda_{ex}/\lambda_{em}$  345 nm/455 nm). The fluorescence densities of nematodes were quantified using computerized image analysis with Olympus cellSens imaging software.

### Calcium imaging

*In vitro* changes in the concentrations of cytoplasmic calcium ( $[Ca^{2+}]_i$ ) can be assessed by measuring the cytoplasmic fluorescence with the calcium indicator Fluo-4 AM (Molecular Probes) [36]. Nematodes were placed on a 2% agarose pad prepared on a glass slide, and then imaged under at 400 magnification on an Olympus BX63 microscope. The excitation and emission wavelengths were 489 nm and 508 nm, respectively. The relative fluorescence (F1/F0) was calculated using computerized image analysis with Olympus cellSens imaging software, where F1

was the fluorescence of *C. elegans* exposed to 63 µg/mL Cry6Aa protein for 6 days or heat stroke, and F0 was the fluorescence of *C. elegans* without Cry6Aa protein or heat stroke [36].

*In vivo* calcium levels were visualized using the calcium indicator d3cpv expressed from the intestine-limited promoter Pnhx-2 in transgenic (rnyEx109) nematodes [42,43]. Nematodes were imaged under Olympus FV1000 inverted confocal IX81 microscope. CFP (405 excitation, 480 emission), and FRET (405 excitation, 535 emission) filters and the FV10-ASW software were used to collect the FRET data. The FRET ratio was calculated by  $(FRET_{int} - FRET_{bkgnd}) / (CFP_{int} - CFP_{bkgnd})$ , where  $FRET_{int}$  and  $CFP_{int}$  represent the fluorescent intensities of the FRET and CFP channels of nematode gut, and  $FRET_{bkgnd}$  and  $CFP_{bkgnd}$  are the fluorescent intensities of FRET and CFP in the background region [41,42].

### Lysosome-like gut granule visualization

*In vitro* lysosomal rupture can be assessed by labeling with lysotracker [43] (Life Technologies, USA). The excitation and emission wavelengths were 555 nm and 580 nm, respectively. *In vivo*, a *C. elegans* transgenic (pwIs50) strain expressing the intestinal lysosomal marker LMP-1::GFP [39,40] was used to examine lysosome integrity. Nematodes were placed on a 2% agarose pad prepared on a glass slide, and then imaged under 400 magnification on an Olympus BX63 microscope. The excitation and emission wavelengths were 489 nm and 508 nm, respectively.

### Nematode heat stroke, hypoxia and propidium iodide staining assays

Nematode heat stroke, hypoxia and propidium iodide staining assays were performed according to the protocol reported by Nikos Kourtis *et al* [35]. Pepstatin A (an aspartyl proteases inhibitor) and Z-Val-Phe-CHO (a calpain inhibitor) were used as necrosis inhibitors [44] in this study. After propidium iodide (Sigma) staining, worms were visualized using an Olympus BX63 microscope. The excitation and emission wavelengths were 555 nm and 580 nm, respectively.

### Statistics

The results presented in each figure are the average of three independent experiments.  $LC_{50}$  values were calculated using PROBIT analysis [69]. The three independent  $LC_{50}$  were averaged and showed as mean  $\pm$  SD. The significance of the differences between two datasets was assessed by Student's *t* test.

### Supporting Information

**S1 Fig. Detection and identification of Cry6Aa binding proteins from *C. elegans* using 2-D electrophoresis and ligand blotting.** For 2-DE, *C. elegans* proteins were resolved by isoelectric focusing using pH 4–7, 18 cm strips followed by separation on an SDS-PAGE gel. Gels were either silver stained (A) or transferred to PVDF filters and probed with biotin-Cry6Aa (B). The positions of molecular size markers (kDa) are indicated on the side of the gel. Arrows denote positions of the major Cry6Aa binding proteins mentioned in the results.

(TIF)

**S2 Fig. Detection of Cry6Aa after ingestion by nematode N2 and *asp-1(tm666)* by Western blot analysis.** N2 and *asp-1(tm666)* were incubated with Cry6Aa protein, and then detected by Western blot using an anti-Cry6Aa antibody. Line 1, Controls of crystal protein Cry6Aa without being incubated by nematode. Line 2, Cry6Aa incubated by wild type N2. Line 3, Cry6Aa incubated by *asp-1(tm666)*.

(TIF)

**S3 Fig. ASP-1-mediated protection of Cry6Aa in *C. elegans*.** (A) The proteolytic digestion of Cry6Aa protoxin (lane 1) by crude protein extracts from wild type nematodes N2 (lane 2), mutant *asp-1(tm666)* (lane 3), Cry6Aa was incubated with ASP-1 (lane 4) or GST (lane 5), and then exposed to extracts from *asp-1(tm666)*. (B) Survival of N2 exposed to Cry6Aa proteolytic digestion in crude protein extracts from N2, mutant *asp-1(tm666)* in the presence or absence of ASP-1. Data were showed as mean  $\pm$  SD (n = 3).

(TIF)

**S4 Fig. The uptake of propidium iodide was significantly suppressed in necrosis mutants *itr-1(sa73)* (A), *tra-3(e1107)* (B), and *vha-12(ok821)* (C) after exposure to Cry6Aa.** These images should be compared to the necrosis induced in wild type N2 from Fig 3. Fluorescence microscopy was used to monitor propidium iodide uptake. One of the fluorescent images were magnified (boxed inset). The numbers of cell corpses per nematode were counted (Right). These results are the mean  $\pm$  SD of three independent experiments. Double asterisks indicate  $p < 0.01$ . The bar denotes 20  $\mu$ m.

(TIF)

**S5 Fig. Intestinal cell plasma membrane integrity was lost in *asp-3(tm4559)* (A), and *asp-4(ok2693)* (B) after exposure to Cry6Aa.** These images should be compared to the necrosis induced in wildtype N2 from Fig 3. Fluorescence microscopy was used to monitor propidium iodide uptake. Arrows indicate intestinal cells stained with propidium iodide due to loss of membrane integrity. One of the fluorescent images were magnified (boxed inset). The numbers of cell corpses per nematode were counted (Right). These results are the mean  $\pm$  SD of three independent experiments. The bar denotes 20  $\mu$ m.

(TIF)

**S6 Fig. Heat stroke results in a burst of death fluorescence in *C. elegans*.** DIC and the fluorescence microscopy of N2 with or without heat stroke. Typical blue fluorescence increased in N2 after exposure to heat stroke. One of three representative experiments is shown. The bar denotes 20  $\mu$ m.

(TIF)

**S7 Fig. ASP-1 is required for the Cry6Aa-induced necrosis pathway.** (A) The effects of ASP-1 on the Cry6Aa-induced burst of death fluorescence. Typical fluorescence increased in N2 but not in *asp-1(tm666)* after exposure to Cry6Aa. The right part shows the quantification of the death fluorescence levels in N2 and *asp-1(tm666)* after exposure to Cry6Aa. These results are the mean  $\pm$  SD of three independent experiments. Double asterisks indicate  $p < 0.01$ . The bar denotes 20  $\mu$ m. (B) The uptake of propidium iodide was significantly suppressed in *asp-1(tm666)* after exposure to Cry6Aa. These images should be compared to the necrosis induced in wild type N2 from Fig 3. Fluorescence microscopy was used to monitor propidium iodide uptake. The numbers of cell corpses per nematode were counted (Right). These results are the mean  $\pm$  SD of three independent experiments. Double asterisks indicate  $p < 0.01$ . The bar denotes 20  $\mu$ m. (C) The effects of ASP-1 on Cry6Aa-induced intestinal cell lysosomal rupture. DIC and the fluorescence microscopy of *asp-1(tm666)* labeled with the intestinal lysosomal marker lysotracker.

(TIF)

**S8 Fig. Cry5Ba did not induce an increase in cytoplasm calcium concentration in *C. elegans*.** Fluorescence microscopy was used to monitor calcium concentration by measuring cytoplasmic fluorescence using the calcium indicator Fluo-4 AM. The right part shows the quantification of the fluorescence levels. Heat stroke was a positive control. These results are

the mean  $\pm$  SD of three independent experiments. A single asterisk indicates  $p < 0.05$ . The bar denotes 20  $\mu\text{m}$ .

(TIF)

**S9 Fig. The susceptibility of apoptosis mutants to Cry6Aa.** Survival of *ced-3(n171)*, *ced-4(n1162)*, and *ced-9(n1950)* apoptosis mutants exposed to Cry6Aa. Data were showed as mean  $\pm$  SD ( $n = 3$ ).

(TIF)

**S10 Fig. The susceptibility of autophagy mutants to Cry6Aa.** Survival of *unc-51(e1189)* and *lgg-1(bp500)* autophagy mutants exposed to Cry6Aa. Data were showed as mean  $\pm$  SD ( $n = 3$ ).

(TIF)

**S11 Fig. The susceptibility of *asp-1(tm666)* to two other death-inducing stimuli, heat stroke and hypoxia.** Survival of *asp-1(tm666)* exposed to heat stroke and hypoxia. Data were showed as mean  $\pm$  SD ( $n = 3$ ).

(TIF)

**S12 Fig. Confocal laser scanning microscope image showed uptake of Cry6Aa toxin into nematode gut cells.** Nematode were fed rhodamine-labeled Cry6Aa toxins, and then imaged using the rhodamine channel to visualize toxin (left panels), the bright-field to visualize the nematode (middle panels) and merged image (right panels). Toxin was detected inside the nematode gut cells, but not in the control (CK). One of three representative experiments is shown. The bar denotes 21.53  $\mu\text{m}$ .

(TIF)

**S1 Table. PMF results and database searches using the Mascot program and NCBIInr database**

(DOC)

**S2 Table. Data analysis of growth assay for *asp-1(tm666)* response to Cry6Aa**

(DOC)

**S3 Table. Data analysis of mortality assay for *asp-1(tm666)*, *itr-1(sa73)*, *tra-3(e1107)*, *vha-12(ok821)*, *asp-3(tm4559)* and *asp-4(ok2693)* response to Cry6Aa.**

(DOC)

**S4 Table. The information of gene and protein mentioned in this study**

(DOC)

## Acknowledgments

We thank Professor Zhengxing Wu and Dr Liwei Qin from Huazhong University of Science and Technology for the technical assistance in *asp-1* gene rescue experiment. We thank Dr Ce Geng for the statistics analysis. We thank Dr Xiaoxia Luo for the technical assistance in nematode RNA extract. We thank Hongwen Du for culturing some worm strains. We thank Professor Mike Adang from University of Georgia for critical comments. We also thank CGC and Shohei Mitani for providing worm strains.

## Author Contributions

Conceived and designed the experiments: FZ MS. Performed the experiments: FZ CC WZ SJ DW ZY JS YD FW XY ZH JL. Analyzed the data: FZ. Contributed reagents/materials/analysis tools: MS. Wrote the paper: FZ DP LR MS.

## References

- Nikoletopoulou V, Markaki M, Palikaras K, Tavernarakis N (2013) Crosstalk between apoptosis, necrosis and autophagy. *Biochim Biophys Acta* 1833: 3448–3459. doi: [10.1016/j.bbamcr.2013.06.001](https://doi.org/10.1016/j.bbamcr.2013.06.001) PMID: [23770045](https://pubmed.ncbi.nlm.nih.gov/23770045/)
- Sridharan H, Upton JW (2014) Programmed necrosis in microbial pathogenesis. *Trends Microbiol* 22: 199–207. doi: [10.1016/j.tim.2014.01.005](https://doi.org/10.1016/j.tim.2014.01.005) PMID: [24565922](https://pubmed.ncbi.nlm.nih.gov/24565922/)
- Mohammad RM, Muqbil I, Lowe L, Yedjou C, Hsu HY, et al. (2015) Broad targeting of resistance to apoptosis in cancer. *Semin Cancer Biol* 35: S78–S103. doi: [10.1016/j.semcancer.2015.03.001](https://doi.org/10.1016/j.semcancer.2015.03.001) PMID: [25936818](https://pubmed.ncbi.nlm.nih.gov/25936818/)
- Chan FK, Luz NF, Moriwaki K (2015) Programmed necrosis in the cross talk of cell death and inflammation. *Annu Rev Immunol* 33: 79–106. doi: [10.1146/annurev-immunol-032414-112248](https://doi.org/10.1146/annurev-immunol-032414-112248) PMID: [25493335](https://pubmed.ncbi.nlm.nih.gov/25493335/)
- Troulinaki K, Tavernarakis N (2012) Necrotic cell death and neurodegeneration: The involvement of endocytosis and intracellular trafficking. *Worm* 1: 176–181. doi: [10.4161/worm.20457](https://doi.org/10.4161/worm.20457) PMID: [24058844](https://pubmed.ncbi.nlm.nih.gov/24058844/)
- Silke J, Rickard JA, Gerlic M (2015) The diverse role of RIP kinases in necroptosis and inflammation. *Nat Immunol* 16: 689–697. doi: [10.1038/ni.3206](https://doi.org/10.1038/ni.3206) PMID: [26086143](https://pubmed.ncbi.nlm.nih.gov/26086143/)
- Martin JB (1999) Molecular basis of the neurodegenerative disorders. *N Engl J Med* 340: 1970–1980. PMID: [10379022](https://pubmed.ncbi.nlm.nih.gov/10379022/)
- Mocarski ES, Kaiser WJ, Livingston-Rosanoff D, Upton JW, Daley-Bauer LP (2014) True grit: programmed necrosis in antiviral host defense, inflammation, and immunogenicity. *J Immunol* 192: 2019–2026. doi: [10.4049/jimmunol.1302426](https://doi.org/10.4049/jimmunol.1302426) PMID: [24563506](https://pubmed.ncbi.nlm.nih.gov/24563506/)
- Helgason E, Okstad OA, Caugant DA, Johansen HA, Fouet A, et al. (2000) *Bacillus anthracis*, *Bacillus cereus*, and *Bacillus thuringiensis*—one species on the basis of genetic evidence. *Appl Environ Microbiol* 66: 2627–2630. PMID: [10831447](https://pubmed.ncbi.nlm.nih.gov/10831447/)
- Pardo-Lopez L, Soberon M, Bravo A (2013) *Bacillus thuringiensis* insecticidal three-domain Cry toxins: mode of action, insect resistance and consequences for crop protection. *FEMS Microbiol Rev* 37: 3–22. doi: [10.1111/j.1574-6976.2012.00341.x](https://doi.org/10.1111/j.1574-6976.2012.00341.x) PMID: [22540421](https://pubmed.ncbi.nlm.nih.gov/22540421/)
- Vachon V, Laprade R, Schwartz JL (2012) Current models of the mode of action of *Bacillus thuringiensis* insecticidal crystal proteins: a critical review. *J Invertebr Pathol* 111: 1–12. doi: [10.1016/j.jip.2012.05.001](https://doi.org/10.1016/j.jip.2012.05.001) PMID: [22617276](https://pubmed.ncbi.nlm.nih.gov/22617276/)
- Adang MJ, Crickmore N, Jurat-Fuentes JL (2014) Diversity of *Bacillus thuringiensis* crystal toxins and mechanism of action. *Adv Insect Phys* 47: 39–87.
- Melo AL, Soccol VT, Soccol CR (2015) *Bacillus thuringiensis*: mechanism of action, resistance, and new applications: a review. *Crit Rev Biotechnol*: 1–10.
- Zhang X, Candas M, Griko NB, Taussig R, Bulla LA Jr. (2006) A mechanism of cell death involving an adenyl cyclase/PKA signaling pathway is induced by the Cry1Ab toxin of *Bacillus thuringiensis*. *Proc Natl Acad Sci U S A* 103: 9897–9902. PMID: [16788061](https://pubmed.ncbi.nlm.nih.gov/16788061/)
- Zhang X, Candas M, Griko NB, Rose-Young L, Bulla LA Jr. (2005) Cytotoxicity of *Bacillus thuringiensis* Cry1Ab toxin depends on specific binding of the toxin to the cadherin receptor BT-R1 expressed in insect cells. *Cell Death Differ* 12: 1407–1416. PMID: [15920532](https://pubmed.ncbi.nlm.nih.gov/15920532/)
- Cappello M, Bungiro RD, Harrison LM, Bischof LJ, Griffiths JS, et al. (2006) A purified *Bacillus thuringiensis* crystal protein with therapeutic activity against the hookworm parasite *Ancylostoma ceylanicum*. *Proc Natl Acad Sci U S A* 103: 15154–15159. PMID: [17005719](https://pubmed.ncbi.nlm.nih.gov/17005719/)
- Zhang F, Peng D, Ye X, Yu Z, Hu Z, et al. (2012) In vitro uptake of 140 kDa *Bacillus thuringiensis* nematocidal crystal proteins by the second stage juvenile of *Meloidogyne hapla*. *PLoS One* 7: e38534. doi: [10.1371/journal.pone.0038534](https://doi.org/10.1371/journal.pone.0038534) PMID: [22737212](https://pubmed.ncbi.nlm.nih.gov/22737212/)
- Li XQ, Wei JZ, Tan A, Aroian RV (2007) Resistance to root-knot nematode in tomato roots expressing a nematocidal *Bacillus thuringiensis* crystal protein. *Plant Biotechnol J* 5: 455–464. PMID: [17451491](https://pubmed.ncbi.nlm.nih.gov/17451491/)
- Li XQ, Tan A, Voegtline M, Bekele S, Chen CS, et al. (2008) Expression of Cry5B protein from *Bacillus thuringiensis* in plant roots confers resistance to root-knot nematode. *Biol Control* 47: 97–102.
- Hui F, Scheib U, Hu Y, Sommer RJ, Aroian RV, et al. (2012) Structure and glycolipid binding properties of the nematocidal protein Cry5B. *Biochemistry* 51: 9911–9921. doi: [10.1021/bi301386q](https://doi.org/10.1021/bi301386q) PMID: [23150986](https://pubmed.ncbi.nlm.nih.gov/23150986/)
- Griffiths JS, Haslam SM, Yang T, Garczynski SF, Mulloy B, et al. (2005) Glycolipids as receptors for *Bacillus thuringiensis* crystal toxin. *Science* 307: 922–925. PMID: [15705852](https://pubmed.ncbi.nlm.nih.gov/15705852/)
- Marroquin LD, Elyassnia D, Griffiths JS, Feitelson JS, Aroian RV (2000) *Bacillus thuringiensis* (Bt) toxin susceptibility and isolation of resistance mutants in the nematode *Caenorhabditis elegans*. *Genetics* 155: 1693–1699. PMID: [10924467](https://pubmed.ncbi.nlm.nih.gov/10924467/)

23. Scott BA, Avidan MS, Crowder CM (2002) Regulation of hypoxic death in *C. elegans* by the insulin/IGF receptor homolog DAF-2. *Science* 296: 2388–2391. PMID: [12065745](#)
24. Nikolettou V, Tavernarakis N (2014) Necrotic cell death in *Caenorhabditis elegans*. *Methods Enzymol* 545: 127–155. doi: [10.1016/B978-0-12-801430-1.00006-8](#) PMID: [25065889](#)
25. Krishnamoorthy M, Jurat-Fuentes JL, McNall RJ, Andacht T, Adang MJ (2007) Identification of novel Cry1Ac binding proteins in midgut membranes from *Heliothis virescens* using proteomic analyses. *Insect Biochem Mol Biol* 37: 189–201. PMID: [17296494](#)
26. Fernandez-Luna MT, Lanz-Mendoza H, Gill SS, Bravo A, Soberon M, et al. (2010) An alpha-amylase is a novel receptor for *Bacillus thuringiensis* ssp. *israelensis* Cry4Ba and Cry11Aa toxins in the malaria vector mosquito *Anopheles albimanus* (Diptera: Culicidae). *Environ Microbiol* 12: 746–757. doi: [10.1111/j.1462-2920.2009.02117.x](#) PMID: [20002140](#)
27. Candas M, Loseva O, Oppert B, Kosaraju P, Bulla LA Jr. (2003) Insect resistance to *Bacillus thuringiensis*: alterations in the indianmeal moth larval gut proteome. *Mol Cell Proteomics* 2: 19–28. PMID: [12601079](#)
28. Tcherepanova I, Bhattacharyya L, Rubin CS, Freedman JH (2000) Aspartic proteases from the nematode *Caenorhabditis elegans*. Structural organization and developmental and cell-specific expression of asp-1. *J Biol Chem* 275: 26359–26369. PMID: [10854422](#)
29. Wei JZ, Hale K, Carta L, Platzer E, Wong C, et al. (2003) *Bacillus thuringiensis* crystal proteins that target nematodes. *Proc Natl Acad Sci U S A* 100: 2760–2765. PMID: [12598644](#)
30. Talaei-Hassanlou R, Bakhshaei R, Hosseini-Navah V, Khorramnezhad A (2013) Effect of midgut proteolytic activity on susceptibility of lepidopteran larvae to *Bacillus thuringiensis* subsp. *Kurstaki*. *Front Physiol* 4: 406. doi: [10.3389/fphys.2013.00406](#) PMID: [24474937](#)
31. Allison K T, Tracy L M, Tori D G, Kimberly M (2013) Use of Necrotic Markers in the *Drosophila* Ovary. *Methods Mol Biol* 1004: 215–228. doi: [10.1007/978-1-62703-383-1\\_16](#) PMID: [23733580](#)
32. Smith TK, Lund EK, Parker ML, Clarke RG, Johnson IT (2004) Allyl-isothiocyanate causes mitotic block, loss of cell adhesion and disrupted cytoskeletal structure in HT29 cells. *Carcinogenesis* 25: 1409–1415. PMID: [15033907](#)
33. Unal Cevik I, Dalkara T (2003) Intravenously administered propidium iodide labels necrotic cells in the intact mouse brain after injury. *Cell Death Differ* 10: 928–929. PMID: [12868000](#)
34. Geng X, Huang C, Qin Y, McCombs JE, Yuan Q, et al. (2012) Hepatitis B virus X protein targets Bcl-2 proteins to increase intracellular calcium, required for virus replication and cell death induction. *Proc Natl Acad Sci U S A* 109: 18471–18476. doi: [10.1073/pnas.1204668109](#) PMID: [23091012](#)
35. Kourtis N, Nikolettou V, Tavernarakis N (2012) Small heat-shock proteins protect from heat-stroke-associated neurodegeneration. *Nature* 490: 213–218. doi: [10.1038/nature11417](#) PMID: [22972192](#)
36. Luke CJ, Pak SC, Askew YS, Naviglia TL, Askew DJ, et al. (2007) An intracellular serpin regulates necrosis by inhibiting the induction and sequelae of lysosomal injury. *Cell* 130: 1108–1119. PMID: [17889653](#)
37. Artal-Sanz M, Samara C, Syntichaki P, Tavernarakis N (2006) Lysosomal biogenesis and function is critical for necrotic cell death in *Caenorhabditis elegans*. *J Cell Biol* 173: 231–239. PMID: [16636145](#)
38. Troulinaki K, Tavernarakis N (2012) Endocytosis and intracellular trafficking contribute to necrotic neurodegeneration in *C. elegans*. *EMBO J* 31: 654–666. doi: [10.1038/emboj.2011.447](#) PMID: [22157748](#)
39. Hinas A, Wright AJ, Hunter CP (2012) SID-5 is an endosome-associated protein required for efficient systemic RNAi in *C. elegans*. *Curr Biol* 22: 1938–1943. doi: [10.1016/j.cub.2012.08.020](#) PMID: [22981770](#)
40. Treusch S, Knuth S, Slaugenhaupt SA, Goldin E, Grant BD, et al. (2004) *Caenorhabditis elegans* functional orthologue of human protein h-mucolin-1 is required for lysosome biogenesis. *Proc Natl Acad Sci U S A* 101: 4483–4488. PMID: [15070744](#)
41. Geng X, Harry BL, Zhou Q, Skeen-Gaar RR, Ge X, et al. (2012) Hepatitis B virus X protein targets the Bcl-2 protein CED-9 to induce intracellular Ca<sup>2+</sup> increase and cell death in *Caenorhabditis elegans*. *Proc Natl Acad Sci U S A* 109: 18465–18470. doi: [10.1073/pnas.1204652109](#) PMID: [23091037](#)
42. Palmer AE, Tsien RY (2006) Measuring calcium signaling using genetically targetable fluorescent indicators. *Nat Protoc* 1: 1057–1065. PMID: [17406387](#)
43. Coburn C, Allman E, Mahanti P, Benedetto A, Cabreiro F, et al. (2013) Anthranilate fluorescence marks a calcium-propagated necrotic wave that promotes organismal death in *C. elegans*. *PLoS Biol* 11: e1001613. doi: [10.1371/journal.pbio.1001613](#) PMID: [23935448](#)
44. Syntichaki P, Xu K, Driscoll M, Tavernarakis N (2002) Specific aspartyl and calpain proteases are required for neurodegeneration in *C. elegans*. *Nature* 419: 939–944. PMID: [12410314](#)

45. Pigott CR, Ellar DJ (2007) Role of receptors in *Bacillus thuringiensis* crystal toxin activity. *Microbiol Mol Biol Rev* 71: 255–281. PMID: [17554045](#)
46. Lettre G, Hengartner MO (2006) Developmental apoptosis in *C. elegans*: a complex CEDnario. *Nat Rev Mol Cell Biol* 7: 97–108. PMID: [16493416](#)
47. Samara C, Syntichaki P, Tavernarakis N (2008) Autophagy is required for necrotic cell death in *Caenorhabditis elegans*. *Cell Death Differ* 15: 105–112. PMID: [17901876](#)
48. Zou CG, Ma YC, Dai LL, Zhang KQ (2014) Autophagy protects *C. elegans* against necrosis during *Pseudomonas aeruginosa* infection. *Proc Natl Acad Sci U S A* 111: 12480–12485. doi: [10.1073/pnas.1405032111](#) PMID: [25114220](#)
49. Xie Z, Klionsky DJ (2007) Autophagosome formation: core machinery and adaptations. *Nat Cell Biol* 9: 1102–1109. PMID: [17909521](#)
50. Ogura K, Wicky C, Magnenat L, Tobler H, Mori I, et al. (1994) *Caenorhabditis elegans* unc-51 gene required for axonal elongation encodes a novel serine/threonine kinase. *Genes Dev* 8: 2389–2400. PMID: [7958904](#)
51. Wong D, Bazopoulou D, Pujol N, Tavernarakis N, Ewbank JJ (2007) Genome-wide investigation reveals pathogen-specific and shared signatures in the response of *Caenorhabditis elegans* to infection. *Genome Biol* 8: R194. PMID: [17875205](#)
52. Wang X, Li Y, Liu S, Yu X, Li L, et al. (2014) Direct activation of RIP3/MLKL-dependent necrosis by herpes simplex virus 1 (HSV-1) protein ICP6 triggers host antiviral defense. *Proc Natl Acad Sci U S A* 111: 15438–15443. doi: [10.1073/pnas.1412767111](#) PMID: [25316792](#)
53. Rodrigue-Gervais IG, Labbe K, Dagenais M, Dupaul-Chicoine J, Champagne C, et al. (2014) Cellular inhibitor of apoptosis protein cIAP2 protects against pulmonary tissue necrosis during influenza virus infection to promote host survival. *Cell Host Microbe* 15: 23–35. doi: [10.1016/j.chom.2013.12.003](#) PMID: [24439895](#)
54. Ruan L, Wang H, Cai G, Peng D, Zhou H, et al. (2015) A two-domain protein triggers heat shock pathway and necrosis pathway both in model plant and nematode. *Environ Microbiol*.
55. Rahman K, Abdullah MA, Ambati S, Taylor MD, Adang MJ (2012) Differential protection of Cry1Fa toxin against *Spodoptera frugiperda* larval gut proteases by cadherin orthologs correlates with increased synergism. *Appl Environ Microbiol* 78: 354–362. doi: [10.1128/AEM.06212-11](#) PMID: [22081566](#)
56. Ruan L, Crickmore N, Peng D, Sun M (2015) Are nematodes a missing link in the confounded ecology of the entomopathogen *Bacillus thuringiensis*? *Trends Microbiol* 23: 341–346. doi: [10.1016/j.tim.2015.02.011](#) PMID: [25818004](#)
57. Huffman DL, Abrami L, Sasik R, Corbeil J, van der Goot FG, et al. (2004) Mitogen-activated protein kinase pathways defend against bacterial pore-forming toxins. *Proc Natl Acad Sci U S A* 101: 10995–11000. PMID: [15256590](#)
58. Kao CY, Los FC, Huffman DL, Wachi S, Kloft N, et al. (2011) Global functional analyses of cellular responses to pore-forming toxins. *PLoS Pathog* 7: e1001314. doi: [10.1371/journal.ppat.1001314](#) PMID: [21408619](#)
59. Brenner S (1974) The genetics of *Caenorhabditis elegans*. *Genetics* 77: 71–94. PMID: [4366476](#)
60. Guo S, Liu M, Peng D, Ji S, Wang P, et al. (2008) New strategy for isolating novel nematocidal crystal protein genes from *Bacillus thuringiensis* strain YBT-1518. *Appl Environ Microbiol* 74: 6997–7001. doi: [10.1128/AEM.01346-08](#) PMID: [18820056](#)
61. Bradford MM (1976) A rapid and sensitive method for the quantitation of microgram quantities of protein utilizing the principle of protein-dye binding. *Anal Biochem* 72: 248–254. PMID: [942051](#)
62. Bischof LJ, Huffman DL, Aroian RV (2006) Assays for toxicity studies in *C. elegans* with Bt crystal proteins. *Methods Mol Biol* 351: 139–154. PMID: [16988432](#)
63. Schrimpf SP, Langen H, Gomes AV, Wahlestedt C (2001) A two-dimensional protein map of *Caenorhabditis elegans*. *Electrophoresis* 22: 1224–1232. PMID: [11358149](#)
64. Mello C, Fire A (1995) DNA transformation. *Methods Cell Biol* 48: 451–482. PMID: [8531738](#)
65. Griffiths JS, Huffman DL, Whitacre JL, Barrows BD, Marroquin LD, et al. (2003) Resistance to a bacterial toxin is mediated by removal of a conserved glycosylation pathway required for toxin-host interactions. *J Biol Chem* 278: 45594–45602. PMID: [12944392](#)
66. Zhang R, Hua G, Andacht TM, Adang MJ (2008) A 106-kDa aminopeptidase is a putative receptor for *Bacillus thuringiensis* Cry11Ba toxin in the mosquito *Anopheles gambiae*. *Biochemistry* 47: 11263–11272. doi: [10.1021/bi801181g](#) PMID: [18826260](#)
67. Ladbury JE, Chowdhry BZ (1996) Sensing the heat: the application of isothermal titration calorimetry to thermodynamic studies of biomolecular interactions. *Chem Biol* 3: 791–801. PMID: [8939696](#)

68. Fragoso RR, Lourenco IT, Batista JA, Oliveira-Neto OB, Silva MC, et al. (2009) *Meloidogyne incognita*: molecular cloning and characterization of a cDNA encoding a cathepsin D-like aspartic proteinase. *Exp Parasitol* 121: 115–123. doi: [10.1016/j.exppara.2008.09.017](https://doi.org/10.1016/j.exppara.2008.09.017) PMID: [18952081](https://pubmed.ncbi.nlm.nih.gov/18952081/)
69. Finney D (1971) Probit analysis. Cambridge, England: University Press.